Journal of Water Process Engineering 71 (2025) 107212

Contents lists available at ScienceDirect

Journal of Water Process Engineering

journal homepage: www.elsevier.com/locate/jwpe

Highly effective antibiotic mineralization via laccase-immobilized nanocomposite beads coupled with fungal phycoremediation

Hilda Dinah Kyomuhimbo [a,*], Usisipho Feleni [b], Hendrik Gideon Brink [a,*]

[a] Department of Chemical Engineering, University of Pretoria, South Africa
[b] Institute for Nanotechnology and Water Sustainability (iNanoWS), College of Science, Engineering and Technology, University of South Africa, South Africa

ARTICLE INFO

Editor: Ludovic F. Dumée

Keywords:
Wastewater treatment
Enzymes
Industrial effluents
Nanoparticles
Polymers

ABSTRACT

This study investigated the synthesis and characterization of laccase (LAC)-activated ZnONPs-CS-PVPP and Ag@ ZnONPs-CS-PVPP composite beads and their application in removal of tetracycline (TET) and ciprofloxacin (CIP). Scanning electron microscopy (SEM) and Transmission electron microscopy (TEM) showed that the doped silver nanoparticles (AgNPs) were spherical globules on the ZnO nanoplates (ZnONPs) and d-spacings of 0.146 nm and 0.148 nm were obtained for ZnONPs and Ag@ ZnONPs respectively. Characterization of composite beads using Fourier transform infrared (FTIR) showed N—H, O—H and C═O stretches responsible for amine, alcohol, carboxylic and amide groups which could be responsible for interaction with the antibiotics during adsorption. Significant removal of antibiotics by enzyme-free and enzyme-enriched beads where 65 % and 72 % removal of TET and 65 % and 60 % removal of CIP were achieved with enzyme free beads. Addition of laccase enzyme to the beads increased the removal of CIP to 85 % for both ZnONPs-CS-PVPP and Ag@ ZnONPs-CS-PVPP beads. LC-MS analysis showed that degradation of TET could be due to hydration of alkene groups followed by elimination of amide, hydroxyl and amine functional groups or ring opening with subsequent hydrolysis or elimination of amide groups. For CIP, decarboxylation and loss of cyclo-propane and diazinane rings as well as fluoride elimination were proposed. Antibiotic activity demonstrated a decrease in activity for CIP through decreased zones of inhibition over time while total loss of growth of *P. aeruginosa* was observed after 1 h degradation of TET. Further mineralization of the degraded byproducts was achieved via phycoremediation using *Aspergillus sp*, demonstrating the potential of this biocatalyst-fungal system for the effective removal of antibiotics from wastewater.

1. Introduction

The extensive production and consumption of antibiotics have resulted in the release of large volumes of antibiotic-containing water, marking them as emerging contaminants [1,2]. Antibiotics serve a diverse array of purposes, spanning from human and animal treatment to their use as feed additives in livestock farming and as ripening agents in agricultural practices [3,4]. Most antibiotics consumed remain unmetabolized and are subsequently discharged into the environment via municipal, agricultural, and industrial wastewater. Conventional wastewater treatment systems are typically not equipped to effectively eliminate these contaminants [5–7]. Antibiotics have been detected in natural environments like river water, groundwater, surface water, and drinking water [8–10].

Antibiotics are persistent in aquatic ecosystems due to their low biodegradability and remain biologically active even at concentrations of ng/L [11,12]. For instance, tetracycline has been detected in wastewater up to 1.42 and 1.54 μ/L in China [13] and Singapore [14] respectively, and 1.29 mg/L in river water in South Africa [15], while ciprofloxacin has been reported in hospital effluent and wastewater treatment plant effluents up to concentrations of 73 μg/L, 31 mg/L and 201 mg/L in Spain [16], India [17] and South Africa [18], respectively. This situation poses various threats, including bioaccumulation in the food chain, the depletion of beneficial bacteria, the emergence of antibiotic-resistant genes (ARGs), which can lead to microbial resistance in pathogenic organisms, and the potential for reactions with other pollutants, resulting in the formation of more stable and toxic products [19,20]. The bio-toxic pressure exerted on diverse aquatic organisms by antibiotics leads to alterations in species distributions, posing harm to the ecosystem as a whole [1,12]. For example, tetracycline inhibits

* Corresponding authors.
E-mail addresses: u21830658@tuks.co.za (H.D. Kyomuhimbo), deon.brink@up.ac.za (H.G. Brink).

https://doi.org/10.1016/j.jwpe.2025.107212
Received 16 December 2024; Received in revised form 29 January 2025; Accepted 6 February 2025
Available online 15 February 2025

protein synthesis [21], and chlortetracycline inhibits the growth of green algae in freshwater systems [22]. Moreover, ciprofloxacin and oxytetracycline form more intricate and toxic mixtures with heavy metals on bacteria and algae than the individual antibiotics [23], and antibiotic resistance to tetracycline increases in the presence of heavy metals like mercury through the induced expression of antibiotic-resistant genes in the presence of the heavy metals [24].

Tetracycline, one of the most widely used class of antibiotics, is difficult to metabolize and up to 80 % gets excreted [25,26]. It is highly soluble in water, difficult to oxidize, has low volatility and easily forms stable compounds due to its binding potential to metal ions [25,27,28]. Similarly, ciprofloxacin is one of the most widely used fluoroquinolone antibiotic in the world especially for the treatment of COVID-19 [29,30]. It has been reported to reduce the removal efficacy of other pollutants such as nitrates and phosphorous [31], and cause body dysfunctions such as blood leukaemia, neurological illnesses, and cardiac dysfunction upon long-term exposure [32]. Therefore, dealing with these antibiotics by either reducing antibiotic consumption or preventing their entry into the environment is of utmost importance. Various techniques have been employed for antibiotic remediation such as adsorption using activated carbon, biochar, and clay [33], membrane processes like microfiltration and ultrafiltration [34], advanced oxidation such as ozonation, photocatalytic, and Fenton process [35], and bioremediation using activated sludge, microbes and enzymes [36]. Bioremediation involving enzymes is promising due to the mild conditions required for enzymatic reactions, minimal sludge production, cost-effective techniques, and these techniques can be employed as tertiary treatments to degrade specific pollutants [37–39].

Laccases are multicopper oxidase enzymes found in fungi, bacteria, and plants and oxidize a wide range of organic substrates while producing water as a by-product [40,41]. Laccases, immobilized on various supports, have gained attention because they require only oxygen to degrade a wide range of organic micropollutants [42,43]. In a bid to obtain a sustainable approach towards the reduction of pollution due to antibiotics, this study explored the use of a two-step elimination of TET and CIP from deionized and wastewater. The first step involved removal using laccase enzyme immobilized on ZnONPs-CS-PVPP and Ag@ZnONPs-CS-PVPP composite beads to break down the antibiotics into smaller by-products. The composites were made from chitosan, polyvinylpolypyrrolidone (PVPP) and zinc oxide or silver-doped zinc oxide nanoparticles. The second step involved complete mineralization of the degradation by-products through phycoremediation using a fungus (*Aspergillus sp*). This process provides a cost-effective approach towards the complete removal of antibiotics from wastewater systems.

2. Materials and methods

Chitosan (medium molecular weight), polyvinylpolypyrrolidone (PVPP), zinc sulphate heptahydrate ($ZnSO_4.7H_2O$, 99 %), silver nitrate (99.8 %), acetic acid (CH_3COOH, 99.9 %), sodium hydroxide (NaOH, 98 %) were obtained from Sigma-Aldrich, South Africa and used without any further purification. Laccase enzyme form *Aspergillus* sp., tetracycline ($C_{22}H_{24}N_2O_8$, 98 %) and Ciprofloxacin ($C_{17}H_{18}FN_3O_3$, 98 %) were obtained from Sigma-Aldrich, USA.

2.1. Synthesis and characterization of composite beads

The synthesis of ZnONPs and Ag@ZnONPs was reported in Kyomuhimbo et al. [44] and the Lac/ZnONPs-CS/PVPP and Lac/Ag@ZnONPs-CS/PVPP beads were synthesized as reported in [45]. Briefly, a mixture solution of 2 % chitosan, PVPP, ZnONPs or Ag@ZnONPs and laccase was prepared in 1.5 % v/v acetic acid while stirring at 400 rpm. The mixture was then dropped in 2 % w/v sodium hydroxide solution using a syringe pump at a distance of 10 cm from the solution. The beads were allowed to cure for 4 h washed with deionized water and stored at 4 °C for further use. Control beads without laccase were also prepared (ZnONPs-CS/PVPP and Ag@ZnONPs-CS/PVPP). The nanoparticles and composite beads were characterized by scanning electron microscopy (SEM) and transmission electron microscopy (TEM).

2.2. Fungal strain identification and characterization

The identification of the fungal species was achieved through the analysis of their genetic material using the internal transcribed spacer (ITS) region of ribosomal DNA (rDNA). The DNA from the cultures was extracted using the Quick-DNA™ Fungal/Bacterial Miniprep Kit (Zymo Research, Catalog No. D6005), and the specific ITS region was replicated using forward ITS1 (5′-TCCGTAGGTGAACCTGCGG-3′) and reverse ITS4 (5′-TCCTCCGCTTATTGATATGC-3′) primers. The PCR process involved a series of steps: an initial heating step of 5 min at 94 °C, followed by 35 cycles of 94 °C for 30 s, 50 °C for 30 s, and 68 °C for 1 min, and a final extension at 68 °C for 10 min. The success of the PCR amplification was confirmed by examining the resulting DNA fragments on a gel (CSL-AG500, stained with EZ-vision Blue light DNA Dye) using the NEB Fast Ladder (N3238) as a size standard. The purified DNA fragments were then prepared for sequencing with the Zymo Research ZR-96 DNA Sequencing Clean-up Kit and sequenced in both forward and reverse directions using the ABI 3730xl Genetic Analyzer (Applied Biosystems, Thermo Fisher Scientific).

To view the raw data from the chromatogram files (.abi), FinchTV was utilized, and the CLC Bio Main Workbench was employed to piece together the forward and reverse sequencing reads into a consensus sequence for each sample. Following this, a BLASTn analysis (with default settings) was conducted on the NCBI website to check if any sequences in the database matched the query sequence above a certain threshold (99 % query coverage; 99 % identity).

2.3. Degradation of antibiotics using beads

Batch degradation experiments were carried out in duplicate on tetracycline and ciprofloxacin dissolved in 5 % v/v acetone and 0.075 % v/v acetic acid respectively with the rest being deionized water (DIW). A 1000 mg/L stock solution of the antibiotics was prepared in acetone and 1.5 % v/v acetic acid for tetracycline and ciprofloxacin respectively and diluted to required concentrations during degradation using DIW. The experiments were carried out at room temperature by adding 1 g of one of the beads (ZnONPs-CS/PVPP, Ag@ZnONPs-CS/PVPP, Lac/ZnONPs-CS/PVPP, Lac/Ag@ZnONPs-CS/PVPP) to 15 mL of 50 mg/L antibiotic solution in 250 mL Erlenmeyer flasks while shaking at 150 rpm. The concentration of tetracycline over degradation time was measured using UV–Vis spectroscopy at a wavelength of 378 nm [46] while that of ciprofloxacin was measured using High-performance liquid chromatography (HPLC). HPLC analysis was performed at 0.5 mL min^{-1} using injection volumes of 10 µL and linear gradient elution of 50 % A (acetonitrile) and 50 % B (DIW) mobile phase at 30 °C.

The adsorption kinetics were studied at room temperature by contacting 1 g of beads with 2.5 mg/L, 5 mg/L, 10 mg/L, 20 mg/L, 50 mg/L and 100 mg/L antibiotics solutions. The equilibrium concentration, C_e (mg/L), was recorded after 24 h and the amount of antibiotics adsorbed onto the beads at equilibrium, Q_e (mg/g) was calculated using the equation;

$$Q_e = (C_o - C_e) \times \frac{V}{m} \quad (1)$$

where, C_o is the initial antibiotic concentration, V is the experimental solution volume and m is the mass of the beads.

2.4. Antibiotic activity of degraded antibiotics

The antibacterial activity of the antibiotics before, during, and after degradation was tested against Gram-positive *Bacillus subtilis* and Gram-

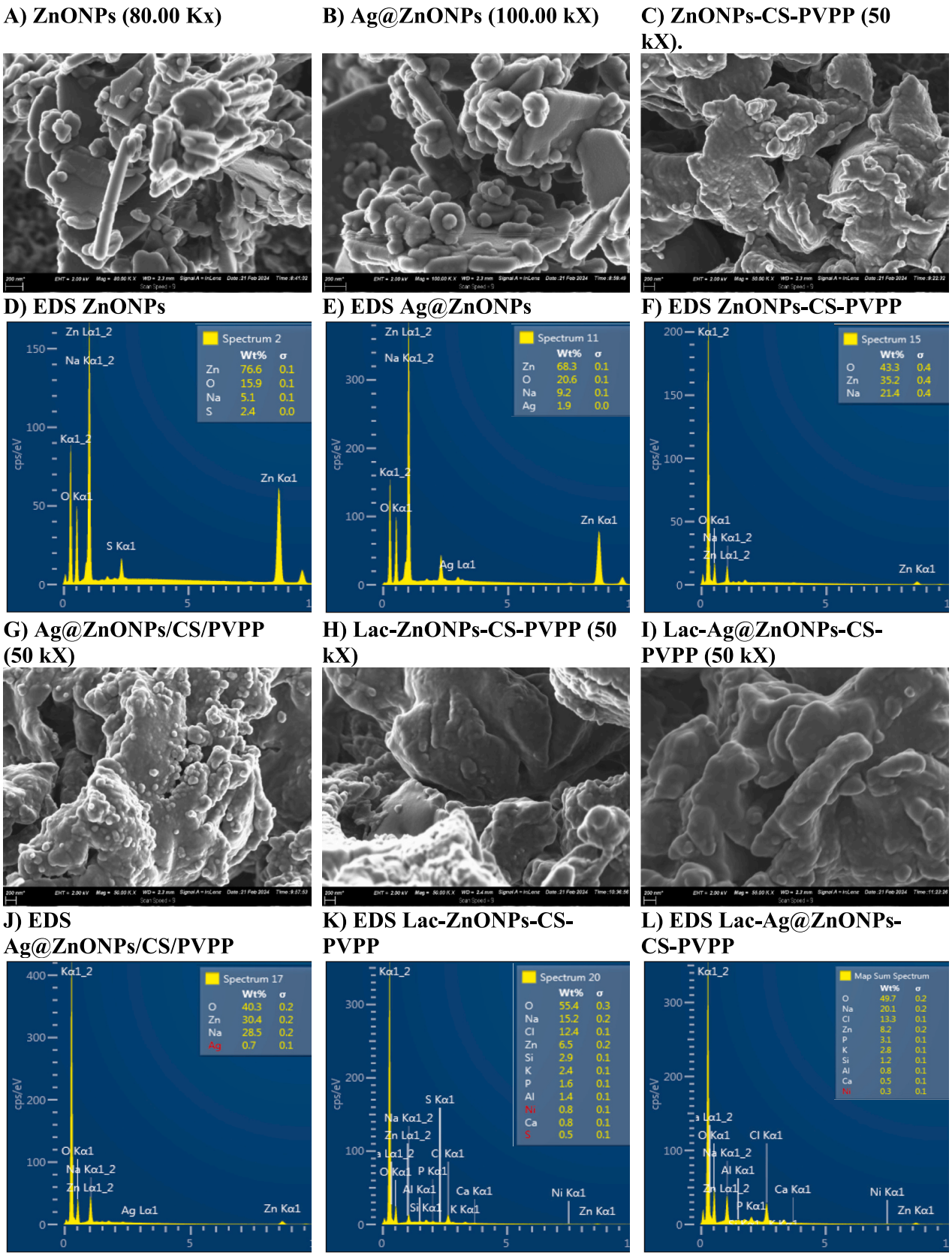

Fig. 1. SEM images of A) ZnONPs, B) Ag@ZnONPs, C) ZnONPs/CS/PVPP, G) Ag@ZnoNPs/CS/PVPP, H) Lac-ZnONPs/CS/PVPP and I) Lac-Ag@ZnONPs/CS/PVPP and EDS of D) ZnONPs, E) Ag@ZnONPs, F) ZnONPs/CS/PVPP, J) Ag@ZnoNPs/CS/PVPP, K) Lac-ZnONPs/CS/PVPP and L) Lac-Ag@ZnONPs/CS/PVPP.

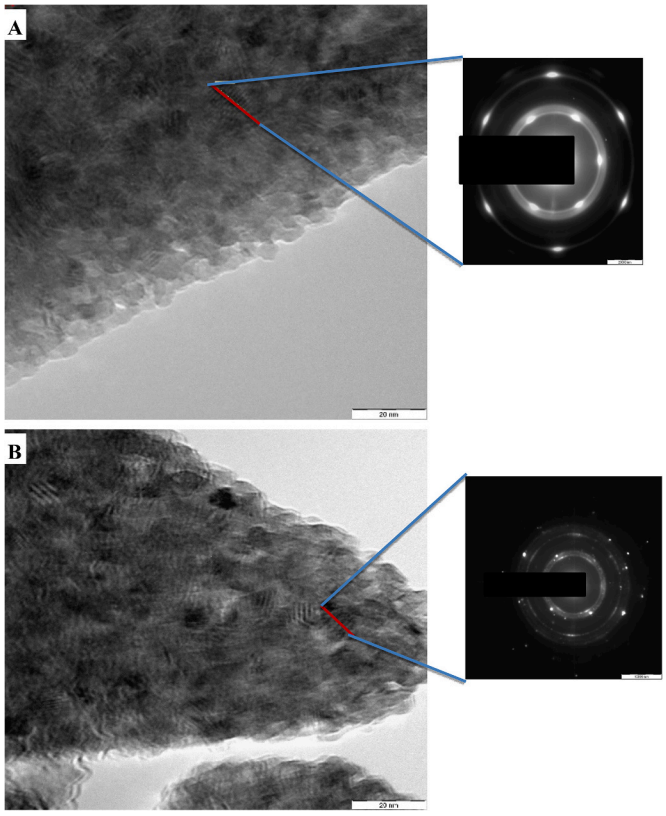

Fig. 2. TEM and SAED for ZnONPs (A) and Ag@ZnONPs (B).

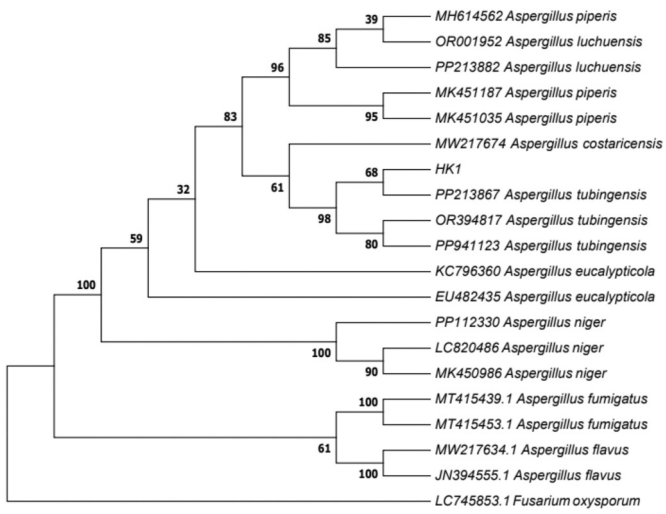

Fig. 3. Molecular phylogenetic analysis of fungal strains.

negative *Pseudomonas aeruginosa* using agar well diffusion assay (for zone of growth inhibition) [47] and (3-(4,5-dimethylthiazol-2-yl)-2,5-diphenyltetrazolium bromide) tetrazolium (MTT) assay (for cellular metabolic activity) [47]. The agar well diffusion assay was carried out by growing the bacteria on nutrient agar in presence of the antibiotics at different stages of degradation. Zones of growth inhibition were measured after 24 h.

The cell metabolic activity of the bacteria was studied using MTT assay. Bacteria were grown in overnight cultures of nutrient broth at a temperature of 37 °C while shaking at 150 rpm until an optical density of OD_{600} = 0.4 was reached. The cultures were centrifuged, and the supernatant was washed twice with deionized water. The supernatant was resuspended in distilled water and the optical density adjusted to approximately OD_{600} = 1. A volume of 1 mL of bacteria was exposed to 2 mL of antibiotic (50 mg/L) in 24 mL broth for 4 h in an incubator at 37 °C while shaking at 200 rpm. A volume of 2.5 mL MTT dye solution (5 mg/mL of MTT in 0.1 M PBS (pH 7.04)) was added to the medium and further exposed for 4 h at 160 RPM in the dark. The absorbance was measured at 570 nm using a VWR UV-1600PC spectrophotometer.

2.5. Mineralization of degraded antibiotic solutions using fungi

The degraded antibiotic solution samples were subjected to phytoremediation using a fungal strain that was accidentally found growing in the degraded samples. The mineralization was carried out in a carbon-limited medium adopted from Juárez-Hernández et al., [48] consisting of 3 g/L D-glucose, 0.66 g/L ammonium tartrate, 0.15 g/L magnesium sulphate heptahydrate, 30 mg/L calcium chloride dihydrate, 5.55 mg/L hydrated iron sulphate and 3.27 mL of 2 N phosphoric acid. Subsequently, 80 mL of culture medium was mixed with 20 mL of degraded antibiotic solution followed by 2 mL of a solution containing 105 spores/mL and incubated at room temperature for 30 days while shaking at 150 rpm. A sample was drawn every 8 days, centrifuged at 10000 rpm for 5 min and the TOC content analyzed. Undegraded antibiotics were used as control samples.

2.6. Application of beads and fungi in wastewater treatment containing antibiotics

To test the applicability of the beads in wastewater treatment, the beads were used to treat sewage wastewater spiked with antibiotics. The wastewater was collected from the Daspoort wastewater treatment facility in Pretoria, South Africa and progressively filtered using membrane filters of 110, 0.45 and 0.22 μm pore sizes. It was spiked with 50 mg/L of TET and CIP and treated with enzyme-free and enzyme-loaded beads and the rate of antibiotic removal was measured. Phytoremediation on the degraded products was also carried out using the fungi on the treated wastewater.

3. Results and discussion

3.1. Characterization of composite beads and fungi

The morphological features of the NPs and nanocomposites were determined using SEM. ZnONPs displayed different agglomerated shapes and sizes (Fig. 1A). The doped NPs displayed globules of spherical Ag particles onto the ZnONPs plates (Fig. 1B). A slight tendency towards aggregation of the nanoparticles was observed which could be due to densification as a result of weak Vander Waal's forces of attraction [49]. The addition of the nanoparticles in the chitosan-PVPP polymers shows agglomerated plates covered in amorphous polymeric layers as shown in Fig. 1C, G–I.

The composition of the NPs and composites was determined using energy-dispersive X-ray spectroscopy (EDS) analysis. The results revealed that the compounds contained elemental Zn and O for ZnONPs and ZnO-based composites and elemental Zn, O and Ag for Ag@ZnONPs and their composites (Fig. 1D–F, J). With the addition of laccase enzyme, other elements including Cl, P, K, Al, Ni and Ca were introduced in the sample (Fig. 1K–L). This could be due to the secondary and tertiary structures of the laccase protein and impurities form the bi-product during laccase production [50]. Two major impurities (S and Na) were identified in the pure NPs. The Na impurity could be due the Na from the reducing agent ($NaBH_4$) that was used during the NPs synthesis and S could be due to the formation of zinc sulphate hydroxide trihydrate intermediate during ZnONPs formation [51].

TEM was used to ascertain the surface morphology of the NPs and determine the crystallinity and interplanar spacing of the NPs. Ring patterns depicting the hexagonal wurtzite structure of crystalline

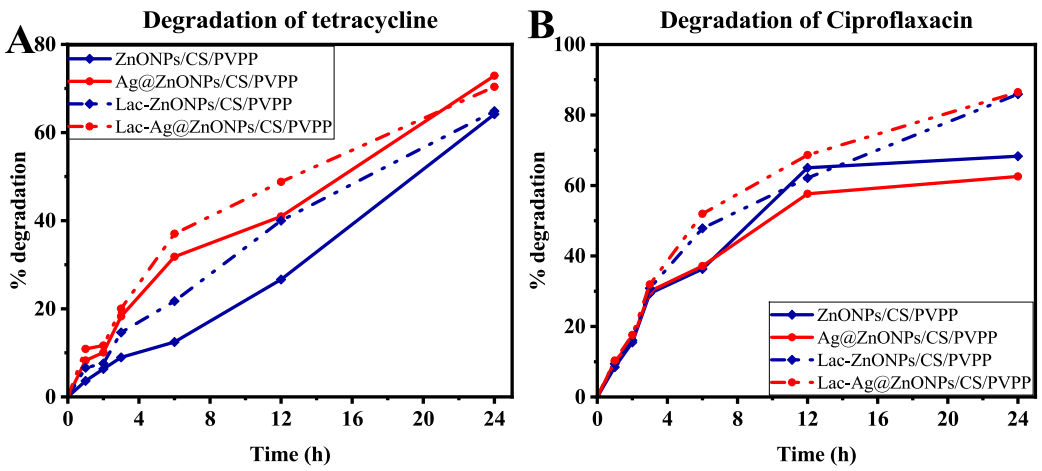

Fig. 4. Degradation of (A) tetracycline and (B) ciprofloxacin using enzyme-free and enzyme-loaded beads.

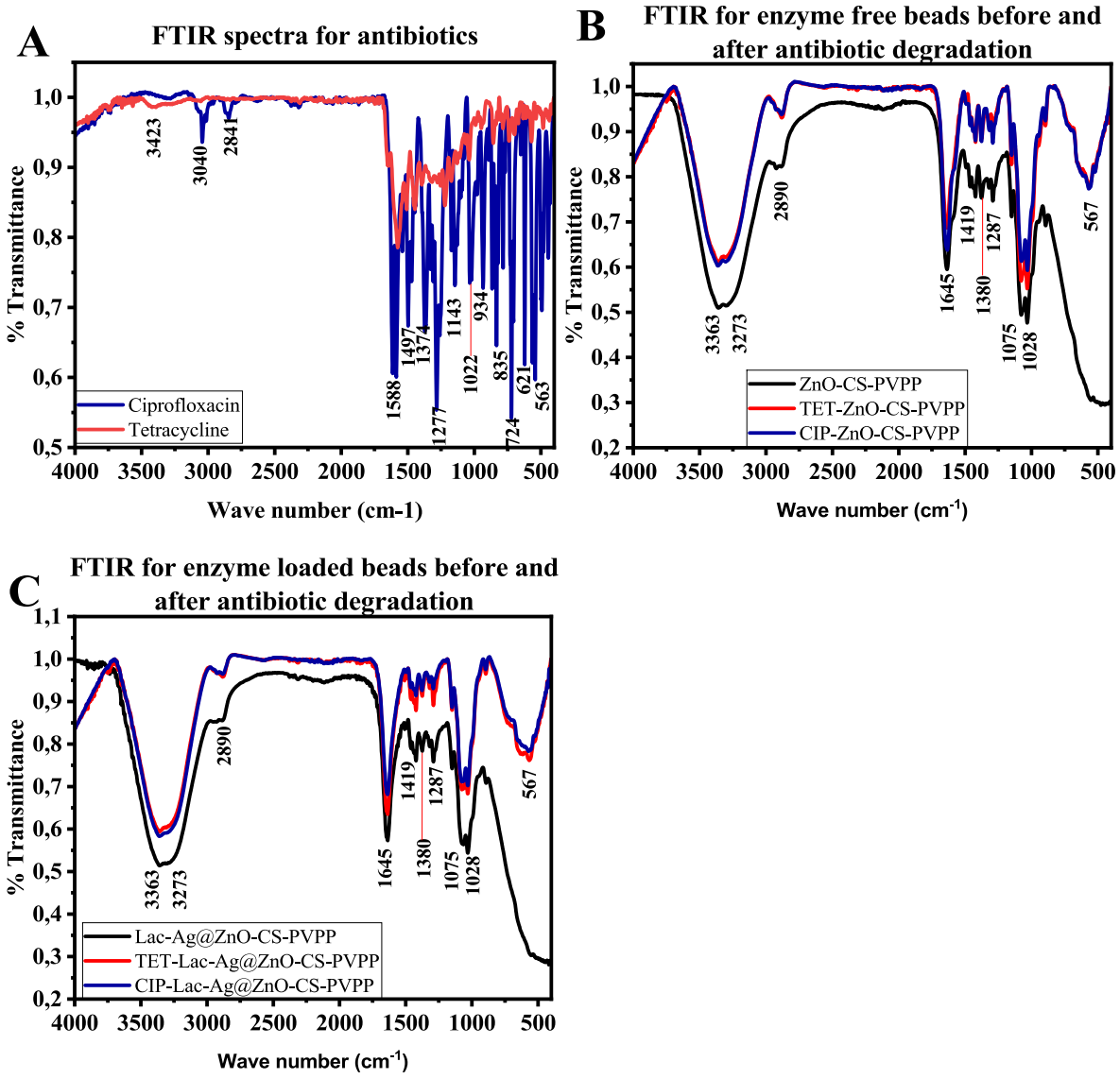

Fig. 5. FTIR spectra for (A) antibiotics, (B) enzyme-free beads before and after antibiotic degradation and (C) enzyme-loaded beads before and after antibiotic degradation.

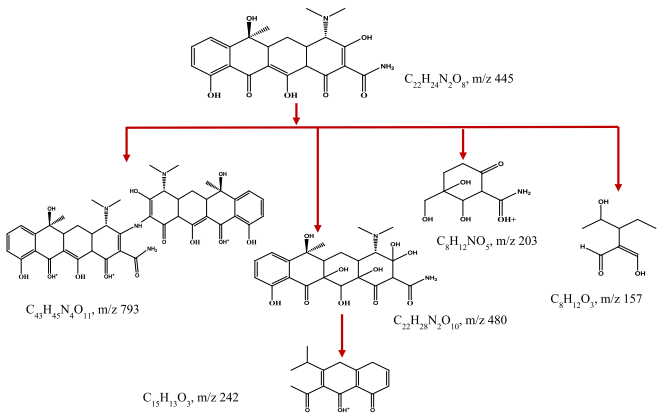

Fig. 6. A schematic representation of the degradation pathway for tetracycline using immobilized laccase beads.

ZnONPs were observed (Fig. 2A). Doping of ZnONPs with Ag increased the tendency to form diffused rings of the sample which could be due to the distribution of Ag particles in their amorphous nature [52] (Fig. 2B). The d-spacing was calculated using Image J software and was obtained as 0.146 nm and 0.148 nm for ZnONPs and Ag@ZnONPs respectively. These interlayer spacings correlated with Braggs reflection angle ($2\theta \sim 70°$) corresponding to the lattice plane (103) that was reported in the XRD results of the same sample by Kyomuhimbo et al., [44].

3.1.1. *Fungal characterization*

The study identified two fungal strains from the Ascomycota phylum and Aspergillus genus. Taxonomic classification was based on molecular characterization and genetic marker analysis. A total of 3 fungal sequences were amplified, ranging from 556 to 602 base pairs (bp) in length. BLASTn analysis confirmed the fungal strains as *Aspergillus niger* (100 % identity) and *Aspergillus tubingensis* (100 % identity), based on pairwise alignment with related GenBank sequences. *A. niger* had a 602 bp sequence length, while *A. tubingensis* had 556 and 602 bp sequences. Phylogenetic analysis of the ITS region of rDNA further confirmed the Aspergillus genus identification, as shown in Fig. 3.

3.2. *Degradation of antibiotics*

Tetracycline, ciprofloxacin, and the chitosan-PVPP polymer complex are rich in amino, hydroxyl, carbonyl and epoxy groups making them hydrophilic. This hydrophilic character in the adsorbent and adsorbate leads to ionic interaction through hydrogen bonding between the hydroxyl and amino functional groups on the antibiotics with the amino, hydroxyl, and carbonyl groups on chitosan and PVPP polymer composite [53–55]. It could also be due to hydrophobic and π-π interactions between the polymers and antibiotics [54,55]. As observed in Fig. 4A and B, there is significant adsorption of the antibiotics on both the enzyme-free and enzyme-enriched beads. For the case of tetracycline, there is no appreciable difference between the removal efficiency for both types of beads over a long time of exposure. At a shorter time, addition of the enzyme to the beads increases the rate of tetracycline removal but it decreases with increased exposure time and the reaction becomes purely adsorption. This could be due to the deactivation of the enzyme by acetone that was used to dissolve the tetracycline [56]. Also, the high adsorption of tetracycline on the beads is attributed to its zwitterionic character in neutral pH which favors the occurrence of hydrogen interactions [57,58]. On the contrary, the addition of laccase enzyme to the beads increases the rate of removal of ciprofloxacin by 20 % from 65 to 85 % (Fig. 4B). The rate of adsorption or degradation is high in the first 12 h due to the abundance of active sites on the beads but slows down in the last 12 h until equilibrium is reached since the active sites are occupied by CIP [59]. For the case of enzyme-loaded beads, the rate of CIP degradation is higher in the first 6 h than in the remaining 18 h.

Fourier transform infrared spectroscopy was carried out on the antibiotics and beads before and after antibiotic degradation to understand the interactions between the beads and antibiotics. Tetracycline (Fig. 5A) displayed bands at 1568 cm^{-1} for N—H bending for amine and C═C stretching for cyclic alkene, 1499 cm^{-1} and 1442 cm^{-1} for C—H bending, 1226 cm^{-1} for O—H bending phenol, 1032 cm^{-1} for C—N stretching amine and 859 cm^{-1} and 744 cm^{-1} for C═C bending alkene [60–63]. On the other hand, CIP produced 2 small bands at 3028 cm^{-1} and 2836 cm^{-1} attributed to C—H stretching alkene and alkane respectively, strong bands at 1588 for N—H bending amine and C═C stretching cyclic alkene, 1497 cm^{-1} and 1368 cm^{-1} for C—H bending alkane methylene and methyl groups respectively, 1281 cm^{-1} for C—N stretching aromatic amine, 1150 cm^{-1} for C—F stretching, 1045 cm^{-1} for C—N stretching, 936 cm^{-1} for C═C bending and 820, 720 and 621 cm^{-1} for C—H bending (Fig. 5B) [64–66].

The enzyme-free and enzyme-loaded composite beads (Fig. 5B–C) displayed more functional groups with a broad double band in the range of 3550–3200 cm^{-1} with tips at 3363 cm^{-1} for N—H stretching due to secondary amine and 3273 cm^{-1} for O—H stretching due to alcohol (intermolecular bonded). A shoulder band at 2890 cm^{-1} could be attributed to O—H stretching of alcohol (intramolecular), the strong band at 1637 cm^{-1} to C═O stretching for amide, 1419 cm^{-1} for O—H bending due to carboxylic acid and/or C—H bending aromatic compound, 1378 cm^{-1} for S═O sulphate stretching, 1287 cm^{-1} for C—O stretching due to aromatic ester, and 1067 cm^{-1} and 1028 cm^{-1} for C—N stretching corresponding to amine [67–69]. After degradation/adsorption of antibiotics on the beads, the bands identified with N—H, O—H stretching at 3363, 3273 and 2890 cm^{-1} showed a slight shift and reduced in intensity. Similarly, the bands corresponding to C—N for amine, C═O for amide and O—H for carboxylic acid significantly reduced their intensity as observed in Fig. 5B–C. The shift and decrease in the intensity of the bands suggest that adsorption on the beads is due to hydrogen bonding and intermolecular forces between amino groups and oxygen-containing functional groups on the antibiotics and adsorption sites [63,70,71]. Since all the bands with N atoms are affected, it suggests that adsorption is due to the interaction between the antibiotics and protonated amino groups in chitosan (beads) [72].

3.2.1. *Possible degradation pathways for the antibiotics*

To clarify the degradation pathway of the antibiotics using immobilized laccase, LC-MS analysis was employed to identify intermediate products in the process and the corresponding mass spectra shown in Figs. 6 and 7. A *m/z* value 445 was observed at retention times of 2.94 and 3.25 min, corresponding to the tetracycline parent compound and its isomer (Fig. 6). Other intermediate compounds with *m/z* values of 793, 480, 242, 203 and 157 were identified at retention times of 5.92, 6.73, 5.08, 0.83 and 2.63 min respectively. The *m/z* values and possible molecular structures of intermediates of tetracycline indicate that intermediates were generated through removal of electrons from tetracycline to generate free radicals that facilitated polymerization and depolymerization reactions such as homocoupling to form *m/z* 793 [73,74], hydration of alkene groups into alcohol to form *m/z* 480 [75,76], followed by elimination of amide, hydroxyl and amine functional groups to form *m/z* 242 [77]. A mechanism involving ring opening with subsequent hydrolysis of the amide group and reduction of the carbonyl to a hydroxyl has been suggested for the formation of *m/z* 203 while for *m/z* 157 [78], ring opening accompanied with elimination of amide, amine groups is suggested [79,80].

A similar phenomenon is observed in the degradation of ciprofloxacin where it underwent homocoupling to form *m/z* 661 followed by substitution of the fluoride group and subsequent hydrolysis to carboxylic acid to form *m/z* 705 (Fig. 7) [81,82]. The formation of *m/z* 245 is attributed to decarboxylation and loss of cyclo-propane while *m/z* 247 is attributed to the loss of the diazinane ring [83,84]. *m/z* 203 and 229

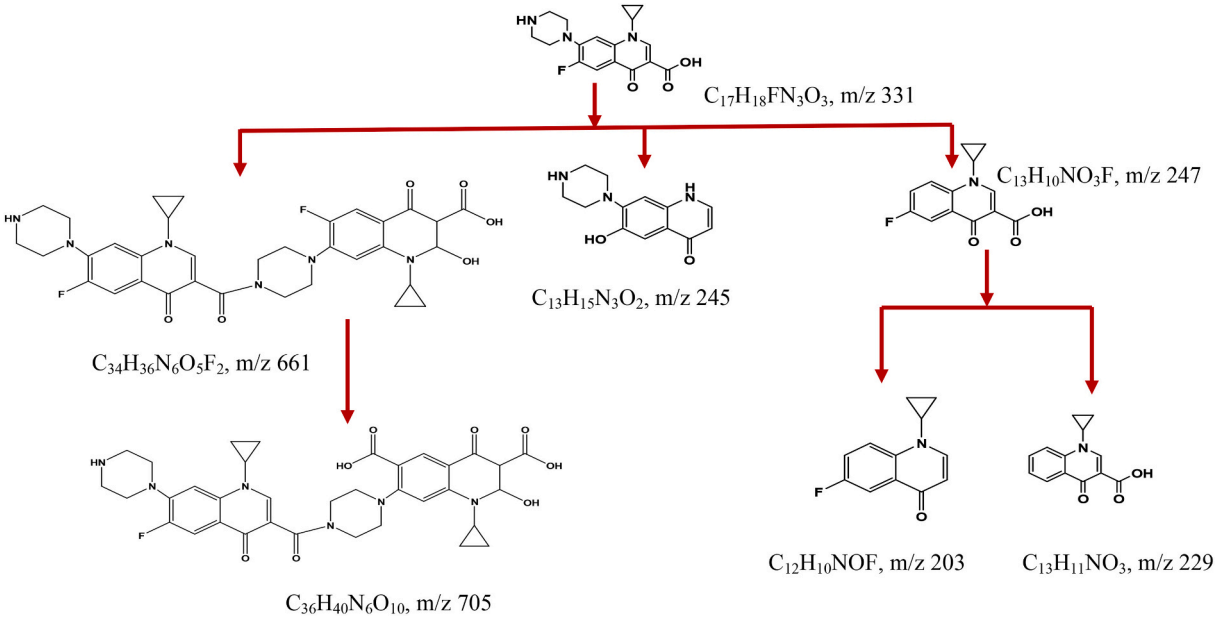

Fig. 7. A schematic representation of the degradation pathway for tetracycline using immobilized laccase beads.

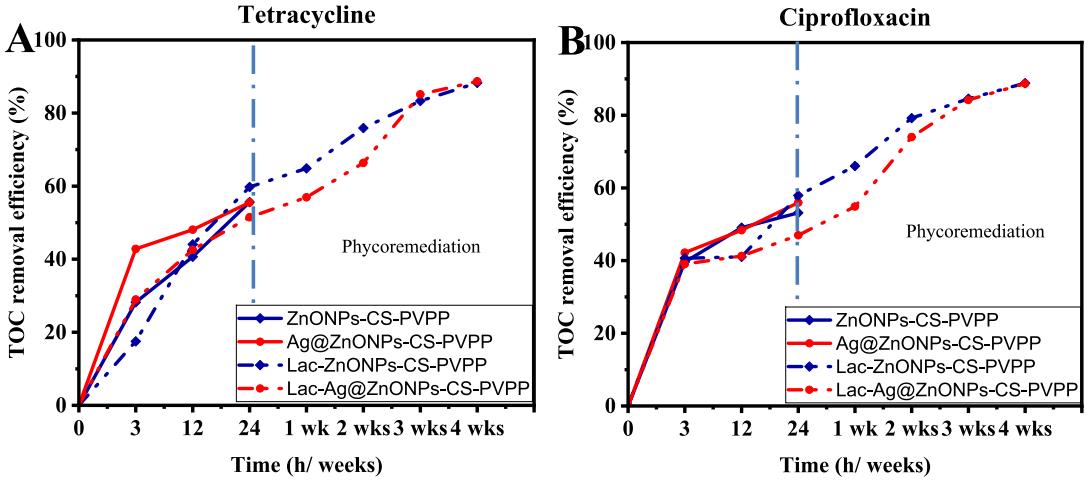

Fig. 8. Total organic carbon of degraded (A) tetracycline and (B) ciprofloxacin. The vertical dash-dotted line indicates the point at which the fungus was introduced.

were attributed to the decarboxylation of *m/z* 247 and fluoride elimination from *m/z* 247 respectively [85,86]. For both cases, the intensity of the parent compound decreased with an increase in degradation time while the intensities of the intermediates remained constant throughout the various degradation times suggesting that complete mineralization of the compounds did not occur.

3.2.2. *Mineralization of degradation byproducts using fungi*

To further assess the degree of mineralization, the total organic carbon of the degraded antibiotics over time was measured using the Photometric Spectroquant TOC cell test from Supelco (1.14878/9.001) and the reduction in TOC with degradation time is presented in Fig. 8A–B. It is worth noting that, although the percentage removal is over 70 % and 85 % for tetracycline and ciprofloxacin respectively, only 60 % of the total organic carbon (TOC) is removed after 24 h for both enzyme-free and enzyme-loaded beads. Moreover, there is no significant difference between the TOC of the antibiotics adsorbed by the free beads and those degraded by the enzyme. This suggests that there was incomplete mineralization of the degradation bi-products as reported by LC-MS analysis.

When fungi and culture media were added to the antibiotic solutions and degradation byproducts, the fungi were observed to grow in the media containing the byproducts. No fungal growth was observed in the undegraded antibiotics over the 30 days, implying that the fungi were feeding on the degradation byproducts rather than the original antibiotic compounds and significant antibiotic removal was observed with the fungi.

TOC analysis conducted at weekly intervals showed further TOC removal of up to 88 % in all the degraded byproduct solutions after 4 weeks. This suggests that the fungi were able to effectively mineralize the degradation byproducts. The level of mineralization is known to depend on the structure of the compound and the type of microorganism involved [87]. Factors such as electron distribution, charge density and type, and the number and position of functional groups in the pollutants can greatly influence the level of removal, with higher molecular weight compounds being harder to remove [88,89]. This could explain why the fungi were able to feed on the degradation byproducts but not the original antibiotic molecules.

LC-MS analysis was carried out on the mineralized samples to confirm removal of the degradation biproducts. For the case of TET,

Table 1
Best fit values for single-site Langmuir, dual-site Langmuir and Freundlich isotherms for degradation of TET and CIP.

Isotherm model	Zn		Ag		L/Zn		L/Ag	
	TET	CIP	TET	CIP	TET	CIP	TET	CIP
Langmuir								
Qm	1.066	2.236	1.417	3.920	2.500	1.758	3.550	1.715
K_L	0.04304	0.02205	0.02445	0.008558	0.02550	0.07831	0.01503	0.08365
Best fit								
R^2	0.9306	0.9484	0.9886	0.9224	0.7514	0.9949	0.9132	0.9950
	0.05727	0.06736	0.009805	0.09330	0.4804	0.009505	0.1485	0.009184
	0.07568	0.08207	0.03131	0.09659	0.2090	0.03083	0.1162	0.03030
	0.07215	0.07825	0.02986	0.09210	0.2090	0.02939	0.1162	0.02889
	−55.14	−53.19	−76.32	−49.28	−33.28	−76.69	−47.37	−77.10
Freundlich								
K_F	0.07281	0.09725	0.05023	0.08804	3.716e-014	0.1542	0.01177	0.1585
n	1.692	1.547	1.411	1.551	0.09500	1.558	0.7055	1.582
Best fit								
R^2	0.8887	0.9756	0.9701	0.9518	0.9366	0.9779	0.9728	0.9742
Sum of Squares	0.09191	0.03183	0.02566	0.05796	0.1225	0.04089	0.04652	0.04774
Sy.x	0.09587	0.05642	0.05065	0.07613	0.1055	0.06394	0.06820	0.06909
RMSE	0.09141	0.05379	0.04829	0.07259	0.1055	0.06097	0.06503	0.06588
AICc	−49.46	−62.19	−64.77	−55.00	−49.68	−59.18	−57.63	−57.32
BET								
Q_m					0.09254		0.2053	
K_S					10.99		2.416	
K_L					0.04797		0.03336	
Best fit								
R^2					0.9757		0.9787	
					0.04704		0.03643	
					0.06261		0.06036	
					0.06540		0.05755	
					−64.10		−60.57	

Table 2
Best fit values for pseudo-first-order (PFO) and pseudo-second-order (PSO) graphs for degradation of TET and CIP.

Kinetic model	Zn		Ag		L/Zn		L/Ag	
Pseudo first order	TET	CIP	TET	CIP	TET	CIP	TET	CIP
Best-fit values								
Qe	0.7475	0.5470	0.5767	0.4819	0.7092	0.6684	0.5711	0.6680
k1	0.04353	0.1412	0.04651	0.1680	0.05796	0.1177	0.09853	0.1347
Goodness of Fit								
R squared	0.9913	0.9779	0.9455	0.9855	0.9541	0.9884	0.9829	0.9914
Sum of Squares	0.003105	0.01068	0.9455	0.005496	0.01992	0.007528	0.007208	0.005993
Sy.x	0.01609	0.02984	0.03004	0.02140	0.04075	0.02505	0.02451	0.02235
RMSE	0.01545	0.02867	0.04632	0.02056	0.03915	0.02406	0.02355	0.02147
AICc	−109.4	−92.10	0.04475	−101.4	−83.37	−96.99	−97.60	−100.2
Pseudo second order								
Best-fit values								
Qe	1.216	0.7228	0.8561	0.6137	1.066	0.9047	0.7963	0.8901
k1	0.02269	0.1694	0.03820	0.2562	0.03886	0.1093	0.09895	0.1296
Goodness of Fit								
R squared	0.9916	0.9704	0.9367	0.9817	0.9568	0.9913	0.9856	0.9903
Sum of Squares	0.002991	0.01430	0.03489	0.006925	0.01873	0.005607	0.006054	0.006751
Sy.x	0.01579	0.03452	0.04992	0.02402	0.03951	0.02162	0.02246	0.02372
RMSE	0.01517	0.03317	0.04823	0.02308	0.03796	0.02077	0.02158	0.02279
AICc	−109.9	−88.01	−90.05	−98.16	−84.23	−101.1	−100.0	−98.52

traces of *m/z* 158 were still observed and a peak for *m/z* 445 corresponding to the parent compound was also observed. For CIP, only the peaks for the parent compound *m/z* 332 and the polymer *m/z* 661 were observed after mineralization implying that all the smaller compounds had been broken down by the fungi. In both samples two new peaks of *m/z* 116 and *m/z* 124 at retention times 0.7 and 8 min have been observed and they could be produced from the fungi.

3.2.3. Adsorption isotherms

Antibiotic solutions of varying concentrations (2.5 mg/L to 100 mg/L) were contacted with 1 g of composite beads at room temperature for 24 h to obtain equilibrium. For the enzyme loaded beads, the beads were autoclaved at 130 °C for 8 h to deactivate the enzyme. The amount of antibiotics removed adsorbed at equilibrium, Q_e (mg/g) was plotted as a function of the equilibrium concentration, C_e (mg/L). To analyze the equilibrium data, three isotherm models namely, Langmuir to identify the adsorptive capacity of the beads, Freundlich for surface heterogeneity and BET to determine surface area of the enzyme loaded beads in multilayer adsorption, were used in their non-linear forms in Eqs. (2), (3) and (4) respectively.

$$Q_e = \frac{Q_m K_L C_e}{1 + K_L C_e} \tag{2}$$

$$Q_e = K_F C_e^{1/n} \tag{3}$$

$$Q_e = \frac{Q_m K_s C_e}{(1 - K_L C_e)(1 - K_L C_e + K_s C_e)} \tag{4}$$

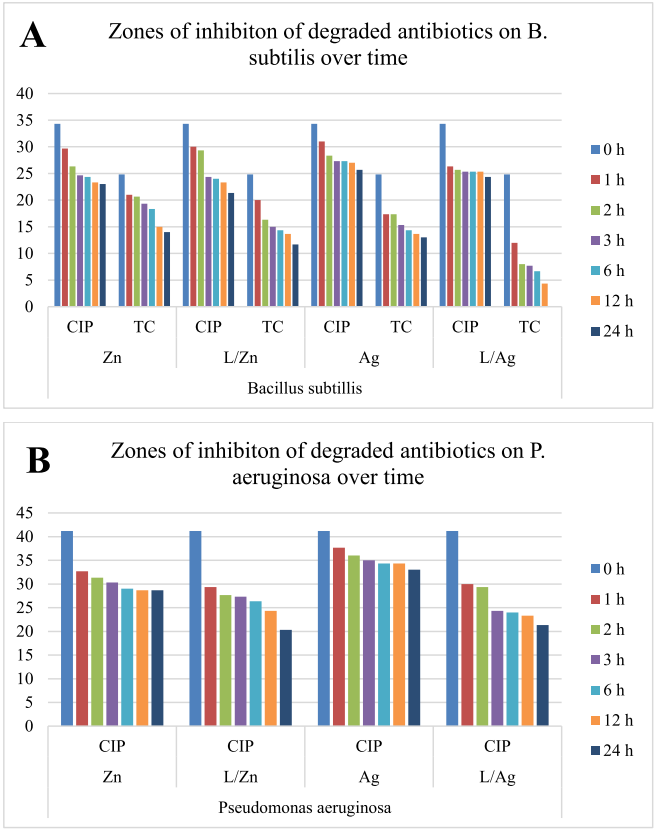

Fig. 9. Antibacterial activity of degraded TET and CIP against (A) *B. subtilis* and (B) *P. aeruginosa*.

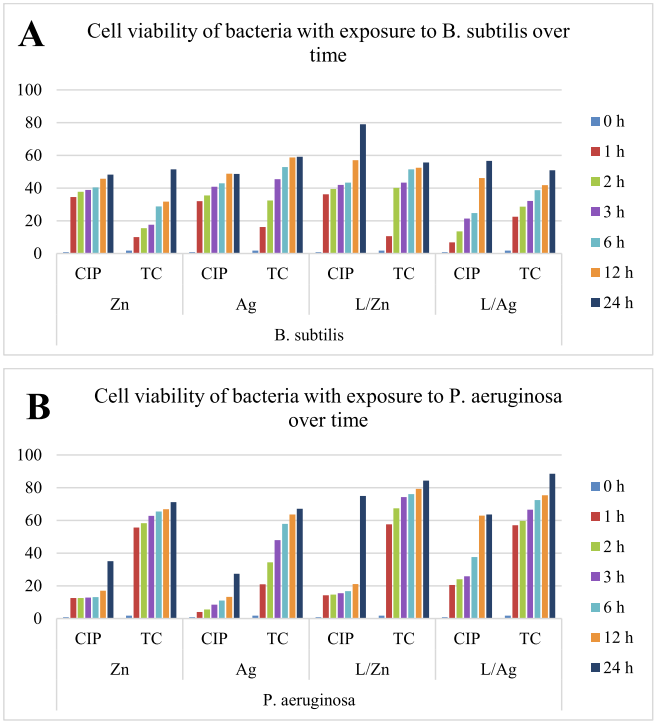

Fig. 10. Effect of degraded TET and CIP on cell metabolic activity on (A) *B. subtilis* and (B) *P. aeruginosa*.

where, Q_m is the monolayer adsorption capacity of the adsorption sites (mg/g), K_L is the Langmuir isotherm /affinity constant for the adsorption site (L/mg) and K_F ((mg/g) $(L/mg)^{1/n}$) and n the adsorption potential and strength constants of the Freundlich isotherm model. The isotherm model parameters were obtained by non-linear regression and the fitting parameters provided in Table 1.

To assess the quality of the model fits to the experimental data, several goodness-of-fit parameters were employed, each providing valuable insights into the model's performance and aiding in the selection of the most appropriate adsorption model. The coefficient of determination (R^2) measures the proportion of variance in the dependent variable that can be explained by the independent variables. A higher R^2 value, approaching 1, indicates a better fit; however, it does not account for overfitting or the number of model parameters, making it potentially misleading when non-linear relationships or outliers are present. The root mean square error (RMSE), on the other hand, quantifies the absolute fit error by representing the square root of the average squared differences between observed and predicted values. Lower RMSE values signify better fit accuracy, yet RMSE is sensitive to large errors and does not provide insights into systematic biases in prediction.

The Akaike Information Criterion (AIC) was also utilized to evaluate model fit while considering complexity, penalizing models with excessive parameters to avoid overfitting. Lower AIC values indicate a better balance between fit and complexity, although it should be used comparatively rather than in isolation. Additionally, the sum of squares (SS) was applied to capture the total variation explained by the model, with the regression sum of squares representing the explained variation and the residual sum of squares (RSS) indicating the unexplained portion. A lower RSS suggests a better fit; however, SS does not account for differences in sample sizes, which can hinder direct model comparisons across different datasets.

Lastly, the standard error of estimate (Sy.x) measures the standard deviation of residuals, offering an estimate of the model's predictive accuracy. While a lower Sy.x implies better fit, it is sensitive to data variability and sample size and is best interpreted alongside other fit metrics. Collectively, a model with high R^2, low RMSE, low AIC, and low Sy.x values is generally considered the most robust. By utilizing multiple goodness-of-fit parameters in combination, the study ensures a comprehensive evaluation of model performance, reducing the risk of misinterpretation and enhancing the reliability of the conclusions drawn.

The Langmuir adsorption isotherm assumes that a monolayer of the adsorbate adsorbs to a homogenous adsorbent surface with uniform energy distribution and no interaction between adsorbed molecules occurs [90–92]. The Freundlich isotherm model assumes multilayer adsorption in which the amount of adsorbed solute per unit adsorbent mass increases gradually [93]. Brunauer-Emmett-Teller (BET) isotherm model assumes multilayer adsorption which occurs after formation of a monolayer followed by layer-by-layer stacking of the next adsorbate layers via adsorbate-adsorbate interaction [94,95].

The adsorption behavior of TET and CIP on enzyme-free and enzyme-loaded beads was evaluated using three isotherm models—Langmuir, Freundlich, and BET—each providing distinct insights into the adsorption mechanisms and surface interactions.

For TET adsorption, the Langmuir model, which assumes monolayer adsorption on a homogenous surface, demonstrated the best fit for enzyme-free beads with the highest R^2 value (0.9886) and the lowest RMSE (0.03131), indicating that adsorption predominantly occurs as a uniform monolayer. The addition of laccase enzyme to the beads led to an increase in the maximum adsorption capacity (Qm), suggesting enhanced adsorption potential. However, for enzyme-loaded beads, the Freundlich model, which accounts for adsorption on heterogeneous surfaces with variable site energies, provided a better fit ($R^2 = 0.9728$) with a lower AIC (−57.63), highlighting the increased complexity of adsorption behavior due to enzyme interactions. The application of the

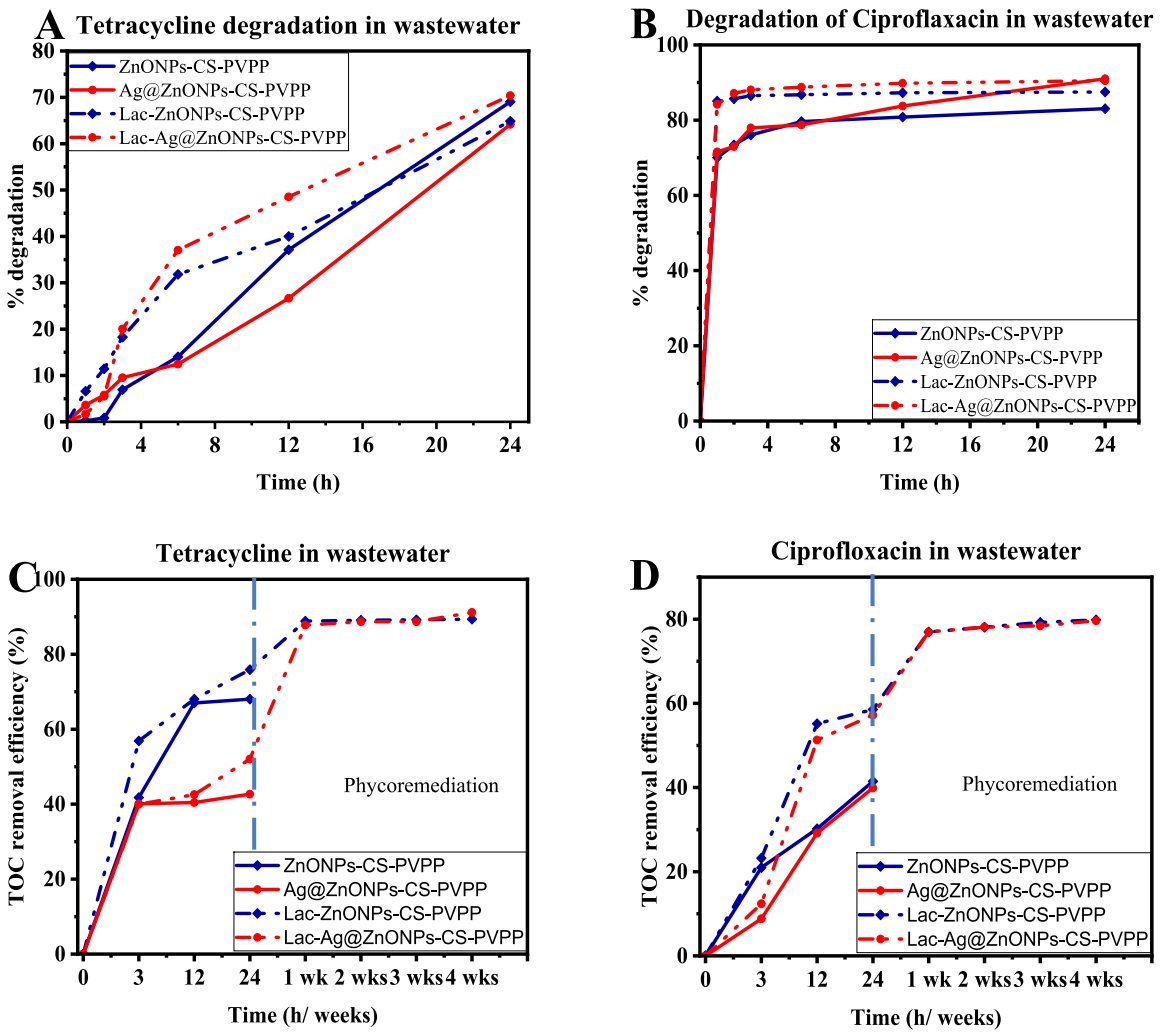

Fig. 11. Time-dependent removal of (A) TET and (B) CIP spiked in sewage wastewater and TOC removal efficiency of (C) TET and (D) CIP spiked in sewage wastewater. The vertical dash-dotted line indicates the point at which the fungus was introduced.

BET model to enzyme-loaded beads further confirmed multilayer adsorption, as reflected by the high R^2 (0.9757) and low AIC (−64.10), indicating a gradual increase in TET uptake and the presence of multilayer adsorption sites.

For CIP adsorption, a different trend was observed. The Freundlich model provided a superior fit for enzyme-free beads (R^2 = 0.9756, AIC = −62.19), suggesting adsorption on heterogeneous surfaces with varying affinities. However, with the addition of laccase enzyme, the Langmuir model exhibited the best fit (R^2 = 0.9950, AIC = −77.10), indicating that enzyme loading resulted in a shift towards monolayer adsorption, with a notable increase in the affinity constant (KL), signifying stronger interactions between CIP and the bead surfaces. Interestingly, despite the lower maximum adsorption capacity (Qm) observed with enzyme addition, the higher affinity constants suggest that the enzyme presence enhances adsorption strength rather than capacity.

The BET model, applied to enzyme-loaded beads for both TET and CIP adsorption, provided critical insights into the multilayer adsorption mechanism. With R^2 values of 0.9757 and 0.9787 for TET and CIP, respectively, and lower RMSE values, the BET model confirmed the presence of multilayer adsorption phenomena, reinforcing the idea that enzyme modification introduces complex adsorption interactions that extend beyond simple monolayer coverage. The gradual increase in adsorption per unit mass of beads, as depicted in Figs. S1 and S2, further supports this interpretation [96].

The combined analysis of the Langmuir, Freundlich, and BET models provides a comprehensive understanding of the adsorption mechanisms. The results demonstrate that enzyme-free beads primarily follow monolayer or heterogeneous adsorption depending on the adsorbate, while enzyme-loaded beads exhibit a more complex multilayer adsorption pattern. The integration of multiple goodness-of-fit parameters, including R^2, RMSE, AIC, sum of squares, and Sy.x, ensures a robust evaluation of model performance and adsorption behavior under different conditions.

3.2.4. *Adsorption kinetics*

To predict the rate of antibiotic removal from the solution and the mechanism of the adsorption process, Lagergren's pseudo-first-order (PFO) [97] and Ho and McKay's pseudo-second-order (PSO) [98] (Eqs. (5) and (6) respectively) were used to fit the kinetics data as shown in Figs. S3–S4.

$$Q_t = Q_e\left(1 - e^{-k_1 t}\right) \tag{5}$$

$$Q_t = \frac{k_2 Q_e^{\,2} t}{1 + k_2 Q_e t} \tag{6}$$

where k_1 (L/h) is the PFO rate constant and k_2 (g/mg/h) is the PFO rate constant. The kinetic parameters for PFO and PSO were obtained by non-linear curve fitting and are summarized in Table 2.

Based on the updated Table 2, the pseudo-first-order (PFO) and pseudo-second-order (PSO) kinetic models were evaluated to understand the adsorption mechanisms of TET and CIP onto enzyme-free and enzyme-loaded beads. The PFO model, which assumes that adsorption occurs through the attachment of a single antibiotic molecule to a single active site on the bead surface, implies that the adsorption rate is directly influenced by the number of vacant sites available. Conversely, the PSO model suggests that adsorption involves a more complex interaction where one antibiotic molecule occupies two adsorption sites on the bead surface, implying a chemisorption process [99,100]. Both kinetic models showed good agreement between the calculated and experimental equilibrium adsorption capacities (Qe), as indicated by the high R^2 values (>0.93), demonstrating that adsorption onto the beads could follow either a pseudo-first or pseudo-second-order mechanism (Figs. S3–S4).

Both kinetic models showed good agreement between the calculated and experimental equilibrium adsorption capacities (Qe), as indicated by the high R^2 values (>0.93), demonstrating that adsorption onto the beads could follow either a pseudo-first or pseudo-second-order mechanism. For TET adsorption, the PSO model provided a slightly better fit with higher R^2 values (up to 0.9916 for enzyme-free beads and 0.9856 for enzyme-loaded beads) compared to the PFO model (up to 0.9913 for enzyme-free beads and 0.9829 for enzyme-loaded beads), suggesting that chemisorption is more dominant in TET adsorption. On the other hand, for CIP adsorption, the PFO model exhibited comparable R^2 values (up to 0.9914), indicating that physical adsorption processes might also contribute significantly.

Additional goodness-of-fit measures, including RMSE and AIC values, were analyzed to validate model performance. Lower RMSE values observed for the PSO model (e.g., 0.01517 for enzyme-free TET adsorption and 0.02077 for enzyme-loaded TET adsorption) compared to the PFO model (e.g., 0.01545 and 0.02355, respectively) further support the suitability of the PSO model for describing the adsorption process. Similarly, lower AIC values for the PSO model (e.g., −109.9 for TET and −98.16 for CIP) compared to the PFO model (e.g., −109.4 and −101.4, respectively) indicate that the PSO model provides a better balance between model complexity and fit quality.

Both PFO and PSO models effectively describe the adsorption kinetics of TET and CIP, with the PSO model exhibiting a slightly better fit, suggesting a chemisorption-dominated process. The inclusion of multiple fit parameters, such as R^2, RMSE, and AIC, ensures a comprehensive evaluation of adsorption kinetics and provides deeper insights into the underlying adsorption mechanisms.

The adsorption of solutes on adsorbents involves 4 major steps, that is, bulk movement (mass transfer) as the adsorbent is dropped in the solution, film diffusion where the solute particles slowly move from the boundary layer to the adsorbent surface, intraparticle movement of solute from larger pores to micropores and lastly, rapid attachment of solute on the active site of the pores [101,102]. In most cases, the film and intraparticle diffusion are the rate-determining steps and can be influenced by stirring speed, size of adsorbent and concentration of solute [102–104].

To describe the mechanism of adsorption of the antibiotics onto the beads, the intra-particle diffusion model [105] and Boyd's single resistance model of film diffusion [106,107] were employed as given by Eqs. (7) and (8) respectively.

$$Q_t = k_p t^{\frac{1}{2}} + C \tag{7}$$

$$-ln\left(1 - \frac{Q_t}{Q_e}\right) = k_{fd} t \tag{8}$$

where k_p (mg/(g.$h^{0.5}$)) is the intra-particle diffusion (IPD) constant and C is a constant (mg/g) that is proportional to the boundary layer thickness and k_{fd} is the adsorption rate constant.

A plot of Qt vs square root of time for all the antibiotics gave multilinear or curvilinear graphs instead of straight lines as shown in Figs. S3–S4. This indicated that the adsorption of the antibiotics onto the beads involves two or more steps contributed by external adsorption followed by gradual IPD. Extrapolation of all the line segments do not pass through the origin implying that IPD is not the sole determinant of the rate-limiting step but IPD and the boundary layer [101,108,109].

Since adsorbate ions move from the liquid phase to the solid adsorbent by crossing a liquid film around the adsorbent, the Boyd model was used to investigate the role played by the liquid film around the beads in the antibiotic adsorption process. A plot of -ln (1-Q_t/Q_e) vs t in all case gave graphs with intercepts implying that the IPD process contributed the rate of adsorption as well [110]. This correlates with the multi-linear IPD graphs indicating that the rate of adsorption is determined by IPD and diffusion of adsorbate through liquid film surrounding the beads [111,112]. The best-of-fit values obtained for TET are 0.987, 0.976, 0.955 and 0.979 while for CIP are 0.941, 0.972, 0.970 and 0.988 for ZnONPs-CS-PVPP, Ag@ ZnONPs-CS-PVPP, Lac- ZnONPs-CS-PVPP and Lac—Ag@ ZnONPs-CS-PVPP respectively. In all cases, the fitting lines did not pass through the origin (Figs. S3–S4) implying that the adsorption of the antibiotics onto the beads involved both IPD and film diffusion. Low intercept values (<1) were also obtained which was indicative of the significance of IPD in the rate of adsorption [113].

3.3. Antibacterial activity of degraded TET and CIP

The antibacterial activity of the antibiotics before, during, and after degradation was tested against Gram-positive *Bacillus subtilis* and Gram-negative *Pseudomonas aeruginosa* using agar well diffusion assay (for zone of growth inhibition) and (3-(4,5-dimethylthiazol-2-yl)-2,5-diphenyltetrazolium bromide) tetrazolium (MTT) assay (for cellular metabolic activity). As observed in Fig. 9, there is a general drop in the efficacy of the antibacterial activity of antibiotics with an increase in degradation time evident in the smaller zones of inhibition for both *B. subtilis* and *P. aeruginosa*. CIP traps gyrases on the DNA to form a CIP-DNA-protein complex which acts as a roadblock to DNA unwinding and replication, blocks DNA synthesis and causes DNA double-strand breaks. As a result, the bacterial cell is poisoned and eventually leads to cell death [114,115]. For the case of CIP, there is no significant difference between the trend of inhibition zones for enzyme-free and enzyme-loaded beads with the final degraded CIP product producing inhibition zone diameters above 20 mm for both bacteria. The large inhibition zones in the enzyme-degraded products could be due to the generation of bacteriostatic bi-products [116].

On the contrary, TET shows a significant decrease in inhibition zones with increased degradation time for the case of *B. subtilis* and total loss of growth inhibition for *P. aeruginosa* even after 1 h of degradation. No zones of inhibition were recorded upon exposure of degraded TET with *P. aeruginosa*. The antibacterial mechanism of TET depends on metal coordination. TET coordinates with Mg^{2+} ions to form $[Mg(TET)]^+$ complex which binds to the bacterial 30S ribosomal subunit thereby blocking the attachment of aminoacyl-tRNA to the ribosome hence inhibiting protein synthesis [117–119]. It also disturbs bacteria cell membrane organization and localization of the peripheral membrane proteins thus causing membrane deformations [120]. Therefore, the drastic decrease of the antibacterial activity of TET upon adsorption onto the enzyme-free beads and degradation with enzyme-loaded beads could be due to the utilization of the active coordination sites on the TET for hydrogen bonding and intermolecular interactions with the OH, amino and C═O functional groups on the beads.

Degradation of the antibiotics with the beads reduces the effect of the antibiotics on the metabolic activity of the bacteria as observed in Fig. 10. Although TET did not inhibit the growth of *P. aeruginosa*, it is evident that the degraded TET has an impact on the metabolic activity of the bacteria meaning that the degradation process only stopped the bacteriostatic and not the bactericidal properties of TET. The addition of the enzyme to the beads causes a significant decrease in the cytotoxicity

of the antibiotics during their degradation implying that laccase immobilized on these composite beads can be used to remedy the antibacterial activity of residual antibiotics in the environment.

3.4. Application of beads in wastewater

To determine the applicability of the beads in wastewater treatment, wastewater was spiked with 50 mg/L of TET and CIP and tested against antibiotic removal using the enzyme-free and enzyme-loaded beads. A similar trend was observed in TET removal like in deionized water where more TET was removed with an increase in time. On the other hand, the removal of CIP occurred within the first hour of exposure to the beads and a higher CIP removal was reported as compared to CIP in deionized water. This could be attributed to the adsorption of other pollutants that act as new adsorption sites, hence increased CIP removal from wastewater [121,122].

A two-step antibiotic removal using the biocatalyst followed by mineralization using the fungus *Aspergillus sp* was carried out on the antibiotics spiked in wastewater (Fig. 11C–D). Further treatment of the enzyme degradation byproducts with fungi gave up to 90 % and 80 % TOC removal for TET and CIP respectively after 28 days.

4. Conclusions

The degradation of aqueous antibiotics, tetracycline (TET) and ciprofloxacin (CIP), using laccase (LAC)-activated ZnONPs-CS-PVPP and Ag@ ZnONPs-CS-PVPP composite beads was investigated. Control experiments with LAC-free beads (ZnONPs-CS-PVPP and Ag@ZnONPs-CS-PVPP) demonstrated up to 65 % and 70 % removal of CIP and TET, respectively, within 24 h. The addition of laccase to form the biocatalyst displayed increased CIP removal efficiency up to 80 % after 24 h for 50 mg/L concentrations. Fourier transform infrared analysis indicated that adsorption on enzyme-free beads occurred via hydrogen bonding and intermolecular interactions between the amino and hydroxyl groups of the beads and the antibiotics. Degradation pathways revealed incomplete mineralization, producing smaller, less toxic compounds and larger polymers through homo- and hetero-coupling reactions. Extended degradation time resulted in decreased antibiotic activity, as shown by reduced zones of inhibition and increased bacterial metabolic activity. Further mineralization was achieved through treatment of the degradation byproducts with the fungus *Aspergillus tubingensis*. The applicability of the beads in wastewater was observed by their high removal of TET (70 %) and CIP (90 %) from sewage wastewater showing that the biocatalyst can be utilized for the removal of antibiotics from wastewater.

CRediT authorship contribution statement

Hilda Dinah Kyomuhimbo: Writing – review & editing, Writing – original draft, Resources, Methodology, Investigation, Funding acquisition, Formal analysis, Data curation, Conceptualization. **Usisipho Feleni:** Writing – review & editing, Validation, Supervision, Software, Project administration. **Hendrik Brink:** Writing – review & editing, Validation, Supervision, Software, Resources, Project administration, Funding acquisition, Conceptualization.

Declaration of competing interest

The authors declare that they have no known competing financial interests or personal relationships that could have appeared to influence the work reported in this paper.

Acknowledgments

This study was funded by the National Research Foundation (NRF) of South Africa [MND210426597525 and CSRP2204204025], Margaret McNamara Education grants and the Schlumberger Foundation Faculty for the Future program. The work was further supported by the Austrian Federal Ministry of Education, Science and Research (BMBWF) through Austria's Agency for Education and Internationalization (OeAD) [Grant numbers: Africa UNINET P056 and P058 as well as APPEAR Project 341]. APPEAR is a program of the Austrian Development Organization.

Appendix A. Supplementary data

Supplementary data to this article can be found online at https://doi.org/10.1016/j.jwpe.2025.107212.

Data availability

Data will be made available on request.

References

[1] A. Bielen, et al., Negative environmental impacts of antibiotic-contaminated effluents from pharmaceutical industries, Water Res. 126 (Dec. 2017) 79–87, https://doi.org/10.1016/j.watres.2017.09.019.
[2] J. Wang, R. Zhuan, Degradation of antibiotics by advanced oxidation processes: an overview, Sci. Total Environ. 701 (Jan. 2020) 135023, https://doi.org/10.1016/j.scitotenv.2019.135023.
[3] D. Akhil, D. Lakshmi, P. Senthil Kumar, D.-V.N. Vo, A. Kartik, Occurrence and removal of antibiotics from industrial wastewater, Environ. Chem. Lett. 19 (2) (Apr. 2021) 1477–1507, https://doi.org/10.1007/s10311-020-01152-0.
[4] H. Shi, J. Ni, T. Zheng, X. Wang, C. Wu, Q. Wang, Remediation of wastewater contaminated by antibiotics. A review, Environ. Chem. Lett. 18 (2) (Mar. 2020) 345–360, https://doi.org/10.1007/s10311-019-00945-2.
[5] A.A.S. Al-Gheethi, J. Lalung, E.A. Noman, J.D. Bala, I. Norli, Removal of heavy metals and antibiotics from treated sewage effluent by bacteria, Clean Techn. Environ. Policy 17 (8) (Dec. 2015) 2101–2123, https://doi.org/10.1007/s10098-015-0968-z.
[6] R. Anjali, S. Shanthakumar, Insights on the current status of occurrence and removal of antibiotics in wastewater by advanced oxidation processes, J. Environ. Manage. 246 (Sep. 2019) 51–62, https://doi.org/10.1016/j.jenvman.2019.05.090.
[7] M. Pirsaheb, H. Hossaini, H. Janjani, Reclamation of hospital secondary treatment effluent by sulfate radicals based–advanced oxidation processes (SR-AOPs) for removal of antibiotics, Microchem. J. 153 (Mar. 2020) 104430, https://doi.org/10.1016/j.microc.2019.104430.
[8] C. Fu, et al., Occurrence and distribution of antibiotics in groundwater, surface water, and sediment in Xiong'an New Area, China, and their relationship with antibiotic resistance genes, Sci. Total Environ. 807 (Feb. 2022) 151011, https://doi.org/10.1016/j.scitotenv.2021.151011.
[9] R. Gothwal, T. Shashidhar, Antibiotic pollution in the environment: a review, CLEAN – Soil Air Water 43 (4) (2015) 479–489, https://doi.org/10.1002/clen.201300989.
[10] N.A. Sabri, et al., Prevalence of antibiotics and antibiotic resistance genes in a wastewater effluent-receiving river in the Netherlands, J. Environ. Chem. Eng. 8 (1) (Feb. 2020) 102245, https://doi.org/10.1016/j.jece.2018.03.004.
[11] G. Lofrano, et al., Photocatalytic degradation of the antibiotic chloramphenicol and effluent toxicity effects, Ecotoxicol. Environ. Saf. 123 (Jan. 2016) 65–71, https://doi.org/10.1016/j.ecoenv.2015.07.039.
[12] B.L. Phoon, et al., Conventional and emerging technologies for removal of antibiotics from wastewater, J. Hazard. Mater. 400 (Dec. 2020) 122961, https://doi.org/10.1016/j.jhazmat.2020.122961.
[13] H.W. Leung, et al., Distribution, fate and risk assessment of antibiotics in sewage treatment plants in Hong Kong, South China, Environ. Int. 42 (Jul. 2012) 1–9, https://doi.org/10.1016/j.envint.2011.03.004.
[14] N.H. Tran, H. Chen, M. Reinhard, F. Mao, K.Y.-H. Gin, Occurrence and removal of multiple classes of antibiotics and antimicrobial agents in biological wastewater treatment processes, Water Res. 104 (Nov. 2016) 461–472, https://doi.org/10.1016/j.watres.2016.08.040.
[15] T.Z. Addis, J.T. Adu, M. Kumarasamy, M. Demlie, Occurrence of trace-level antibiotics in the Msunduzi River: an investigation into South African environmental pollution, Antibiotics 13 (2) (Feb. 2024) 2, https://doi.org/10.3390/antibiotics13020174.
[16] K. Oberlé, M.-J. Capdeville, T. Berthe, H. Budzinski, F. Petit, Evidence for a complex relationship between antibiotics and antibiotic-resistant Escherichia coli: from medical center patients to a receiving environment, Environ. Sci. Technol. 46 (3) (Feb. 2012) 1859–1868, https://doi.org/10.1021/es203399h.
[17] D.G.J. Larsson, C. de Pedro, N. Paxeus, Effluent from drug manufactures contains extremely high levels of pharmaceuticals, J. Hazard. Mater. 148 (3) (Sep. 2007) 751–755, https://doi.org/10.1016/j.jhazmat.2007.07.008.
[18] E. Holton, E. Archer, J. Fidal, T. Kjeldsen, G. Wolfaardt, B. Kasprzyk-Hordern, Spatiotemporal urban water profiling for the assessment of environmental and public exposure to antimicrobials (antibiotics, antifungals, and antivirals) in the Eerste River Catchment, South Africa, Environ. Int. 164 (Jun. 2022) 107227, https://doi.org/10.1016/j.envint.2022.107227.

[19] X. Liu, et al., Insight into electro-Fenton and photo-Fenton for the degradation of antibiotics: mechanism study and research gaps, Chem. Eng. J. 347 (Sep. 2018) 379–397, https://doi.org/10.1016/j.cej.2018.04.142.
[20] M. Milaković, et al., Effects of industrial effluents containing moderate levels of antibiotic mixtures on the abundance of antibiotic resistance genes and bacterial community composition in exposed creek sediments, Sci. Total Environ. 706 (Mar. 2020) 136001, https://doi.org/10.1016/j.scitotenv.2019.136001.
[21] J. Wang, R. Zhuan, L. Chu, The occurrence, distribution and degradation of antibiotics by ionizing radiation: an overview, Sci. Total Environ. 646 (Jan. 2019) 1385–1397, https://doi.org/10.1016/j.scitotenv.2018.07.415.
[22] L.-H. Yang, G.-G. Ying, H.-C. Su, J.L. Stauber, M.S. Adams, M.T. Binet, Growth-inhibiting effects of 12 antibacterial agents and their mixtures on the freshwater microalga Pseudokirchneriella subcapitata, Environ. Toxicol. Chem. 27 (5) (2008) 1201–1208, https://doi.org/10.1897/07-471.1.
[23] Y. Zhang, X. Cai, X. Lang, X. Qiao, X. Li, J. Chen, Insights into aquatic toxicities of the antibiotics oxytetracycline and ciprofloxacin in the presence of metal: complexation versus mixture, Environ. Pollut. 166 (Jul. 2012) 48–56, https://doi.org/10.1016/j.envpol.2012.03.009.
[24] Y. Zhou, Y.-B. Xu, J.-X. Xu, X.-H. Zhang, S.-H. Xu, Q.-P. Du, Combined toxic effects of heavy metals and antibiotics on a Pseudomonas fluorescens strain ZY2 isolated from swine wastewater, Int. J. Mol. Sci. 16 (2) (Feb. 2015) 2, https://doi.org/10.3390/ijms16022839.
[25] F. Ahmad, D. Zhu, J. Sun, Environmental fate of tetracycline antibiotics: degradation pathway mechanisms, challenges, and perspectives, Environ. Sci. Eur. 33 (1) (May 2021) 64, https://doi.org/10.1186/s12302-021-00505-y.
[26] N. Magesh, A. Annam Renita, P. Senthil Kumar, Practice on treating pharmaceutical compounds (antibiotics) present in wastewater using biosorption techniques with different biowaste compounds. A review, Environ. Prog. Sustain. Energy 39 (6) (2020) e13429, https://doi.org/10.1002/ep.13429.
[27] X. He, T. Kai, P. Ding, Heterojunction photocatalysts for degradation of the tetracycline antibiotic: a review, Environ. Chem. Lett. 19 (6) (Dec. 2021) 4563–4601, https://doi.org/10.1007/s10311-021-01295-8.
[28] A. Pal, P. Mahamallik, S. Saha, A. Majumdar, Degradation of tetracycline antibiotics by advanced oxidation processes: application of MnO2 nanomaterials, Nat. Resour. Eng. 2 (1) (Jan. 2017) 32–42, https://doi.org/10.1080/23802693.2018.1434397.
[29] A.K. Al-Buriahi, M.M. Al-shaibani, R.M.S.R. Mohamed, A.A. Al-Gheethi, A. Sharma, N. Ismail, Ciprofloxacin removal from non-clinical environment: a critical review of current methods and future trend prospects, J. Water Process Eng. 47 (Jun. 2022) 102725, https://doi.org/10.1016/j.jwpe.2022.102725.
[30] C. Nepfumbada, N.H. Mthombeni, R. Sigwadi, R.F. Ajayi, U. Feleni, B.B. Mamba, Functionalities of electrochemical fluoroquinolone sensors and biosensors, Environ. Sci. Pollut. Res. 31 (3) (Dec. 2023) 3394–3412, https://doi.org/10.1007/s11356-023-30223-2.
[31] K. Yi, et al., Effect of ciprofloxacin on biological nitrogen and phosphorus removal from wastewater, Sci. Total Environ. 605–606 (Dec. 2017) 368–375, https://doi.org/10.1016/j.scitotenv.2017.06.215.
[32] R. Shen, Y. Yu, R. Lan, R. Yu, Z. Yuan, Z. Xia, The cardiovascular toxicity induced by high doses of gatifloxacin and ciprofloxacin in zebrafish, Environ. Pollut. 254 (Nov. 2019) 112861, https://doi.org/10.1016/j.envpol.2019.07.029.
[33] D. Mangla, A. Sharma, S. Ikram, Critical review on adsorptive removal of antibiotics: present situation, challenges and future perspective, J. Hazard. Mater. 425 (Mar. 2022) 127946, https://doi.org/10.1016/j.jhazmat.2021.127946.
[34] N. Nasrollahi, V. Vatanpour, A. Khataee, Removal of antibiotics from wastewaters by membrane technology: limitations, successes, and future improvements, Sci. Total Environ. 838 (Sep. 2022) 156010, https://doi.org/10.1016/j.scitotenv.2022.156010.
[35] Z. Li, J. Wang, J. Chang, B. Fu, H. Wang, Insight into advanced oxidation processes for the degradation of fluoroquinolone antibiotics: removal, mechanism, and influencing factors, Sci. Total Environ. 857 (Jan. 2023) 159172, https://doi.org/10.1016/j.scitotenv.2022.159172.
[36] M. Apreja, A. Sharma, S. Balda, K. Kataria, N. Capalash, P. Sharma, Antibiotic residues in environment: antimicrobial resistance development, ecological risks, and bioremediation, Environ. Sci. Pollut. Res. 29 (3) (Jan. 2022) 3355–3371, https://doi.org/10.1007/s11356-021-17374-w.
[37] R. Abejón, M. De Cazes, M.P. Belleville, J. Sanchez-Marcano, Large-scale enzymatic membrane reactors for tetracycline degradation in WWTP effluents, Water Res. 73 (Apr. 2015) 118–131, https://doi.org/10.1016/j.watres.2015.01.012.
[38] M. Bilal, S.S. Ashraf, D. Barceló, H.M.N. Iqbal, Biocatalytic degradation/redefining 'removal' fate of pharmaceutically active compounds and antibiotics in the aquatic environment, Sci. Total Environ. 691 (Nov. 2019) 1190–1211, https://doi.org/10.1016/j.scitotenv.2019.07.224.
[39] E. Méndez, M.A. González-Fuentes, G. Rebollar-Perez, A. Méndez-Albores, E. Torres, Emerging pollutant treatments in wastewater: cases of antibiotics and hormones, J. Environ. Sci. Health Part A 52 (3) (Feb. 2017) 235–253, https://doi.org/10.1080/10934529.2016.1253391.
[40] H.D. Kyomuhimbo, H.G. Brink, Applications and immobilization strategies of the copper-centred laccase enzyme; a review, Heliyon 9 (2) (Feb. 2023) e13156, https://doi.org/10.1016/j.heliyon.2023.e13156.
[41] S.H. Khatami, O. Vakili, A. Movahedpour, Z. Ghesmati, H. Ghasemi, M. Taheri-Anganeh, Laccase: various types and applications, Biotechnol. Appl. Biochem. 69 (6) (2022) 2658–2672, https://doi.org/10.1002/bab.2313.
[42] S. Ahmad, W. Sebai, M.-P. Belleville, N. Brun, A. Galarneau, J. Sanchez-Marcano, Experimental and modeling of tetracycline degradation in water in a flow-through enzymatic monolithic reactor, Environ. Sci. Pollut. Res. 29 (50) (Oct. 2022) 75896–75906, https://doi.org/10.1007/s11356-022-21204-y.
[43] M. Harguindeguy, C. Pochat-Bohatier, J. Sanchez-Marcano, M.-P. Belleville, Enzymatic degradation of tetracycline by *Trametes versicolor* laccase in a fluidized bed reactor, Sci. Total Environ. 907 (Jan. 2024) 168152, https://doi.org/10.1016/j.scitotenv.2023.168152.
[44] Hilda Dinah Kyomuhimbo, Evans M.N. Chirwa, Usisipho Feleni, Hendrik Gideon Brink, Zinc oxide and silver doped zinc oxide nanoparticle-chitosan-PVPP composite beads for immobilization of laccase enzyme, in: Proceedings of the Global Congress of Chemical Engineering, South Africa, 2024 (pp. in press).
[45] Hilda Dinah Kyomuhimbo, Evans M.N. Chirwa, Usisipho Feleni, Hendrik Brink, Immobilization of laccase enzyme on zinc oxide and silver doped zinc oxide nanoparticle-chitosan-PVPP composite beads, CET 110 (2024) 373–378, https://doi.org/10.3303/CET24110063.
[46] Q. Shang, N. Liu, D. You, Q. Cheng, G. Liao, Z. Pan, The application of Ni and Cu-MOFs as highly efficient catalysts for visible light-driven tetracycline degradation and hydrogen production, J. Mater. Chem. C 9 (1) (2021) 238–248, https://doi.org/10.1039/D0TC04733C.
[47] A. López-Malo, E. Mani-López, P.M. Davidson, E. Palou, Methods for activity assay and evaluation of results, in: Antimicrobials in Food, 4th ed., CRC Press, 2020.
[48] J. Juárez-Hernández, et al., Isolation of fungi from a textile industry effluent and the screening of their potential to degrade industrial dyes, J. Fungi 7 (10) (Oct. 2021) 10, https://doi.org/10.3390/jof7100805.
[49] K. Elumalai, S. Velmurugan, Green synthesis, characterization and antimicrobial activities of zinc oxide nanoparticles from the leaf extract of *Azadirachta indica* (L.), Appl. Surf. Sci. 345 (Aug. 2015) 329–336, https://doi.org/10.1016/j.apsusc.2015.03.176.
[50] M. Fu, J. Xing, Z. Ge, Preparation of laccase-loaded magnetic nanoflowers and their recycling for efficient degradation of bisphenol A, Sci. Total Environ. 651 (Feb. 2019) 2857–2865, https://doi.org/10.1016/j.scitotenv.2018.10.145.
[51] E. Keleş Güner, R. Akkaş, A. Özer, Synthesis of zinc sulfate hydroxide trihydrate by chemical precipitation and its transformation to zinc oxide, Chem. Eng. Commun. 209 (9) (Sep. 2022) 1203–1213, https://doi.org/10.1080/00986445.2021.1953486.
[52] A.N. Mallika, A. RamachandraReddy, K. SowriBabu, K. Venugopal Reddy, Synthesis and optical characterization of aluminum doped ZnO nanoparticles, Ceram. Int. 40 (8, Part A) (Sep. 2014) 12171–12177, https://doi.org/10.1016/j.ceramint.2014.04.057.
[53] E.F. Durán-Lara, et al., Experimental and theoretical binding affinity between polyvinylpolypyrrolidone and selected phenolic compounds from food matrices, Food Chem. 168 (Feb. 2015) 464–470, https://doi.org/10.1016/j.foodchem.2014.07.048.
[54] E.M. Abd El-Monaem, et al., Sustainable adsorptive removal of antibiotic residues by chitosan composites: an insight into current developments and future recommendations, Arab. J. Chem. 15 (5) (May 2022) 103743, https://doi.org/10.1016/j.arabjc.2022.103743.
[55] M. Gil, et al., Rosé wine fining using polyvinylpolypyrrolidone: colorimetry, targeted polyphenomics, and molecular dynamics simulations, J. Agric. Food Chem. 65 (48) (Dec. 2017) 10591–10597, https://doi.org/10.1021/acs.jafc.7b04461.
[56] A.M. Othman, E. González-Domínguez, Á. Sanromán, M. Correa-Duarte, D. Moldes, Immobilization of laccase on functionalized multiwalled carbon nanotube membranes and application for dye decolorization, RSC Adv. 6 (115) (2016) 114690–114697, https://doi.org/10.1039/C6RA18283F.
[57] F. da Silva Bruckmann, et al., Highly efficient adsorption of tetracycline using chitosan-based magnetic adsorbent, Polymers 14 (22) (Jan. 2022) 22, https://doi.org/10.3390/polym14224854.
[58] F.G. Nunes Filho, E.C. Silva Filho, J.A. Osajima, A.P. de Melo Alves, M.G. Fonseca, Adsorption of tetracycline using chitosan–alginate–bentonite composites, Appl. Clay Sci. 239 (Jul. 2023) 106952, https://doi.org/10.1016/j.clay.2023.106952.
[59] M.Z. Afzal, X.-F. Sun, J. Liu, C. Song, S.-G. Wang, A. Javed, Enhancement of ciprofloxacin sorption on chitosan/biochar hydrogel beads, Sci. Total Environ. 639 (Oct. 2018) 560–569, https://doi.org/10.1016/j.scitotenv.2018.05.129.
[60] Z. Ouyang, F. Lei, E. Hu, S. Li, Q. Yao, X. Guo, New insight into transformation of tetracycline in presence of Mn(II): oxidation versus photolysis, Environ. Pollut. 300 (May 2022) 118998, https://doi.org/10.1016/j.envpol.2022.118998.
[61] Z. Ouyang, et al., Chromate(VI)-induced homogeneous oxidation and photolysis of aqueous tetracycline: kinetics and mechanism, Chem. Eng. J. 379 (Jan. 2020) 122276, https://doi.org/10.1016/j.cej.2019.122276.
[62] H. Wu, H. Xie, G. He, Y. Guan, Y. Zhang, Effects of the pH and anions on the adsorption of tetracycline on iron-montmorillonite, Appl. Clay Sci. 119 (Jan. 2016) 161–169, https://doi.org/10.1016/j.clay.2015.08.001.
[63] B. Yang, et al., Interactions between the antibiotic tetracycline and humic acid: examination of the binding sites, and effects of complexation on the oxidation of tetracycline, Water Res. 202 (Sep. 2021) 117379, https://doi.org/10.1016/j.watres.2021.117379.
[64] E. Mohsen, O.M. El-Borady, M.B. Mohamed, I.S. Fahim, Synthesis and characterization of ciprofloxacin loaded silver nanoparticles and investigation of their antibacterial effect, J. Radiat. Res. Appl. Sci. 13 (1) (Jan. 2020) 416–425, https://doi.org/10.1080/16878507.2020.1748941.
[65] H.S. Rathore, et al., Fabrication and characterization of chitosan film impregnated ciprofloxacin drug: a comparative study, Biocatal. Agric. Biotechnol. 18 (Mar. 2019) 101078, https://doi.org/10.1016/j.bcab.2019.101078.
[66] U.E. Osonwa, J.I. Ugochukwu, E.E. Ajaegbu, K.I. Chukwu, R.B. Azevedo, C. O. Esimone, Enhancement of antibacterial activity of ciprofloxacin hydrochloride

by complexation with sodium cholate, Bull. Fac. Pharm. Cairo Univ. 55 (2) (Dec. 2017) 233–237, https://doi.org/10.1016/j.bfopcu.2017.09.006.
[67] W. Zhang, et al., Preparation of superabsorbent polymer gel based on PVPP and its application in water-holding in sandy soil, J. Environ. Chem. Eng. 9 (6) (Dec. 2021) 106760, https://doi.org/10.1016/j.jece.2021.106760.
[68] B.P. Sudatta, V. Sugumar, R. Varma, P. Nigariga, Extraction, characterization and antimicrobial activity of chitosan from pen shell, Pinna bicolor, Int. J. Biol. Macromol. 163 (Nov. 2020) 423–430, https://doi.org/10.1016/j.ijbiomac.2020.06.291.
[69] W. Zhang, J. Cao, W. Jiang, Analysis of film-forming properties of chitosan with different molecular weights and its adhesion properties with different postharvest fruit surfaces, Food Chem. 395 (Nov. 2022) 133605, https://doi.org/10.1016/j.foodchem.2022.133605.
[70] N. Roy, K. Kannabiran, A. Mukherjee, Studies on photocatalytic removal of antibiotics, ciprofloxacin and sulfamethoxazole, by Fe3O4-ZnO-chitosan/alginate nanocomposite in aqueous systems, Adv. Powder Technol. 33 (8) (Aug. 2022) 103691, https://doi.org/10.1016/j.apt.2022.103691.
[71] H. Zhu, T. Chen, J. Liu, D. Li, Adsorption of tetracycline antibiotics from an aqueous solution onto graphene oxide/calcium alginate composite fibers, RSC Adv. 8 (5) (2018) 2616–2621, https://doi.org/10.1039/C7RA11964J.
[72] J. Kang, H. Liu, Y.-M. Zheng, J. Qu, J.P. Chen, Systematic study of synergistic and antagonistic effects on adsorption of tetracycline and copper onto a chitosan, J. Colloid Interface Sci. 344 (1) (Apr. 2010) 117–125, https://doi.org/10.1016/j.jcis.2009.11.049.
[73] T. Kudanga, B. Nemadziva, M. Le Roes-Hill, Laccase catalysis for the synthesis of bioactive compounds, Appl. Microbiol. Biotechnol. 101 (1) (Jan. 2017) 13–33, https://doi.org/10.1007/s00253-016-7987-5.
[74] K. Sun, S. Li, Y. Si, Q. Huang, Advances in laccase-triggered anabolism for biotechnology applications, Crit. Rev. Biotechnol. 41 (7) (Oct. 2021) 969–993, https://doi.org/10.1080/07388551.2021.1895053.
[75] I. Bassanini, E.E. Ferrandi, S. Riva, D. Monti, Biocatalysis with laccases: an updated overview, Catalysts 11 (1) (Jan. 2021) 1, https://doi.org/10.3390/catal11010026.
[76] E. Brenna, et al., Biocatalytic synthesis of chiral cyclic γ-oxoesters by sequential C–H hydroxylation, alcohol oxidation and alkene reduction, Green Chem. 19 (21) (2017) 5122–5130, https://doi.org/10.1039/C7GC02215H.
[77] N. Najafabadipour, S. Mojtabavi, H. Jafari-Nodoushan, N. Samadi, M. A. Faramarzi, High efficiency of osmotically stable laccase for biotransformation and micro-detoxification of levofloxacin in the urea-containing solution: catalytic performance and mechanism, Colloids Surf. B Biointerfaces 207 (Nov. 2021) 112022, https://doi.org/10.1016/j.colsurfb.2021.112022.
[78] K.K. Navada, A. Kulal, Enhanced production of laccase from gamma irradiated endophytic fungus: a study on biotransformation kinetics of aniline blue and textile effluent decolourisation, J. Environ. Chem. Eng. 8 (2) (Apr. 2020) 103550, https://doi.org/10.1016/j.jece.2019.103550.
[79] A. Sharma, K.K. Jain, A. Jain, M. Kidwai, R.C. Kuhad, Bifunctional in vivo role of laccase exploited in multiple biotechnological applications, Appl. Microbiol. Biotechnol. 102 (24) (Dec. 2018) 10327–10343, https://doi.org/10.1007/s00253-018-9404-8.
[80] K.K. Navada, G. Sanjeev, A. Kulal, Enhanced biodegradation and kinetics of anthraquinone dye by laccase from an electron beam irradiated endophytic fungus, Int. Biodeterior. Biodegrad. 132 (Aug. 2018) 241–250, https://doi.org/10.1016/j.ibiod.2018.04.012.
[81] A.C. Sousa, M. Conceição Oliveira, L.O. Martins, M.P. Robalo, A sustainable synthesis of asymmetric phenazines and phenoxazinones mediated by CotA-laccase, Adv. Synth. Catal. 360 (3) (2018) 575–583, https://doi.org/10.1002/adsc.201701228.
[82] Y. Huang, J. Yang, Kinetics and mechanisms for sulfamethoxazole transformation in the phenolic acid-laccase (Trametes versicolor) system, Environ. Sci. Pollut. Res. 29 (42) (Sep. 2022) 62941–62951, https://doi.org/10.1007/s11356-022-20281-3.
[83] D. Zhu, et al., Insight into depolymerization mechanism of bacterial laccase for lignin, ACS Sustain. Chem. Eng. 8 (34) (Aug. 2020) 12920–12933, https://doi.org/10.1021/acssuschemeng.0c03457.
[84] H. Zhang, et al., Enhancing lignin model compound depolymerization using mediator-enzyme catalysis: a sustainable approach to C–C bond cleavage, ACS Sustain. Chem. Eng. 12 (15) (Apr. 2024) 5842–5849, https://doi.org/10.1021/acssuschemeng.3c07773.
[85] F. Lorquin, et al., Production and properties of non-cytotoxic pyomelanin by laccase and comparison to bacterial and synthetic pigments, Sci. Rep. 11 (1) (Apr. 2021) 8538, https://doi.org/10.1038/s41598-021-87328-2.
[86] A. Aljawish, I. Chevalot, C. Paris, L. Muniglia, Green synthesis of glyco-phenol by enzymatic coupling between ferulic acid and glucosamine: an ecofriendly procedure, Biotechnol. Appl. Biochem. 69 (4) (2022) 1438–1450, https://doi.org/10.1002/bab.2215.
[87] C. Wang, et al., Structure-dependent surface catalytic degradation of cephalosporin antibiotics on the aged polyvinyl chloride microplastics, Water Res. 206 (Nov. 2021) 117732, https://doi.org/10.1016/j.watres.2021.117732.
[88] S.N. Singh, S. Mishra, N. Jauhari, Degradation of anthroquinone dyes stimulated by fungi, in: S.N. Singh (Ed.), Microbial Degradation of Synthetic Dyes in Wastewaters, Springer International Publishing, Cham, 2015, pp. 333–356, https://doi.org/10.1007/978-3-319-10942-8_15.
[89] M.H. Abdurahman, A.Z. Abdullah, N.F. Shoparwe, A comprehensive review on sonocatalytic, photocatalytic, and sonophotocatalytic processes for the degradation of antibiotics in water: synergistic mechanism and degradation pathway, Chem. Eng. J. 413 (Jun. 2021) 127412, https://doi.org/10.1016/j.cej.2020.127412.
[90] X. Guo, J. Wang, Comparison of linearization methods for modeling the Langmuir adsorption isotherm, J. Mol. Liq. 296 (Dec. 2019) 111850, https://doi.org/10.1016/j.molliq.2019.111850.
[91] K.L. Muedi, H.G. Brink, V. Masindi, J.P. Maree, Effective removal of arsenate from wastewater using aluminium enriched ferric oxide-hydroxide recovered from authentic acid mine drainage, J. Hazard. Mater. 414 (Jul. 2021) 125491, https://doi.org/10.1016/j.jhazmat.2021.125491.
[92] S. Alafnan, A. Awotunde, G. Glatz, S. Adjei, I. Alrumaih, A. Gowida, Langmuir adsorption isotherm in unconventional resources: applicability and limitations, J. Petrol. Sci. Eng. 207 (Dec. 2021) 109172, https://doi.org/10.1016/j.petrol.2021.109172.
[93] H.-K. Chung, W.-H. Kim, J. Park, J. Cho, T.-Y. Jeong, P.-K. Park, Application of Langmuir and Freundlich isotherms to predict adsorbate removal efficiency or required amount of adsorbent, J. Ind. Eng. Chem. 28 (Aug. 2015) 241–246, https://doi.org/10.1016/j.jiec.2015.02.021.
[94] H.K. Agbovi, L.D. Wilson, 1 - adsorption processes in biopolymer systems: fundamentals to practical applications, in: S. Kalia (Ed.), Natural Polymers-Based Green Adsorbents for Water Treatment, Elsevier, 2021, pp. 1–51, https://doi.org/10.1016/B978-0-12-820541-9.00011-9.
[95] A. Ebadi, J.S. Soltan Mohammadzadeh, A. Khudiev, What is the correct form of BET isotherm for modeling liquid phase adsorption? Adsorption 15 (1) (Feb. 2009) 65–73, https://doi.org/10.1007/s10450-009-9151-3.
[96] C. Wen, et al., Biochar as the effective adsorbent to combustion gaseous pollutants: preparation, activation, functionalization and the adsorption mechanisms, Prog. Energy Combust. Sci. 99 (Nov. 2023) 101098, https://doi.org/10.1016/j.pecs.2023.101098.
[97] S.K. Lagergren, About the theory of so-called adsorption of soluble substances, Sven Vetenskapsakad Handingarl 24 (1898) 1–39.
[98] Y.S. Ho, G. McKay, Pseudo-second order model for sorption processes, Process Biochem. 34 (5) (Jul. 1999) 451–465, https://doi.org/10.1016/S0032-9592(98)00112-5.
[99] M. Wu, et al., Competitive adsorption of antibiotic tetracycline and ciprofloxacin on montmorillonite, Appl. Clay Sci. 180 (Nov. 2019) 105175, https://doi.org/10.1016/j.clay.2019.105175.
[100] V.O. Shikuku, R. Zanella, C.O. Kowenje, F.F. Donato, N.M.G. Bandeira, O. D. Prestes, Single and binary adsorption of sulfonamide antibiotics onto iron-modified clay: linear and nonlinear isotherms, kinetics, thermodynamics, and mechanistic studies, Appl Water Sci 8 (6) (Sep. 2018) 175, https://doi.org/10.1007/s13201-018-0825-4.
[101] G.W. Kajjumba, et al., Modelling of adsorption kinetic processes—errors, theory and application, in: Advanced Sorption Process Applications, IntechOpen, 2018, https://doi.org/10.5772/intechopen.80495.
[102] C. Yao, T. Chen, A film-diffusion-based adsorption kinetic equation and its application, Chem. Eng. Res. Des. 119 (Mar. 2017) 87–92, https://doi.org/10.1016/j.cherd.2017.01.004.
[103] F.-C. Wu, R.-L. Tseng, R.-S. Juang, Initial behavior of intraparticle diffusion model used in the description of adsorption kinetics, Chem. Eng. J. 153 (1) (Nov. 2009) 1–8, https://doi.org/10.1016/j.cej.2009.04.042.
[104] H. Zhang, L. Chen, M. Lu, J. Li, L. Han, A novel film–pore–surface diffusion model to explain the enhanced enzyme adsorption of corn stover pretreated by ultrafine grinding, Biotechnol. Biofuels 9 (1) (Aug. 2016) 181, https://doi.org/10.1186/s13068-016-0602-2.
[105] W.J. Weber, J.C. Morris, Kinetics of adsorption on carbon from solution, J. Sanit. Eng. Div. 89 (2) (Apr. 1963) 31–59, https://doi.org/10.1061/JSEDAI.0000430.
[106] G.E. Boyd, A.W. Adamson, L.S. Myers, The exchange adsorption of ions from aqueous solutions by organic zeolites. II. Kinetics [1], J. Am. Chem. Soc. 69 (11) (Nov. 1947) 2836–2848, https://doi.org/10.1021/ja01203a066.
[107] D. Reichenberg, Properties of ion-exchange resins in relation to their structure. III. Kinetics of exchange, J. Am. Chem. Soc. 75 (3) (Feb. 1953) 589–597, https://doi.org/10.1021/ja01099a022.
[108] W. Xiang, et al., Adsorption of tetracycline hydrochloride onto ball-milled biochar: governing factors and mechanisms, Chemosphere 255 (Sep. 2020) 127057, https://doi.org/10.1016/j.chemosphere.2020.127057.
[109] H.M. Jang, S. Yoo, Y.-K. Choi, S. Park, E. Kan, Adsorption isotherm, kinetic modeling and mechanism of tetracycline on *Pinus taeda*-derived activated biochar, Bioresour. Technol. 259 (Jul. 2018) 24–31, https://doi.org/10.1016/j.biortech.2018.03.013.
[110] W. Duan, N. Wang, W. Xiao, Y. Zhao, Y. Zheng, Ciprofloxacin adsorption onto different micro-structured tourmaline, halloysite and biotite, J. Mol. Liq. 269 (Nov. 2018) 874–881, https://doi.org/10.1016/j.molliq.2018.08.051.
[111] S.A. Chaudhry, T.A. Khan, I. Ali, Equilibrium, kinetic and thermodynamic studies of Cr(VI) adsorption from aqueous solution onto manganese oxide coated sand grain (MOCSG), J. Mol. Liq. 236 (Jun. 2017) 320–330, https://doi.org/10.1016/j.molliq.2017.04.029.
[112] R.M.C. Viegas, M. Campinas, H. Costa, M.J. Rosa, How do the HSDM and Boyd's model compare for estimating intraparticle diffusion coefficients in adsorption processes, Adsorption 20 (5) (Aug. 2014) 737–746, https://doi.org/10.1007/s10450-014-9617-9.
[113] J. Yao, Y. Deng, D.-S. Li, H. Li, H.Y. Yang, Role of magnetic substances in adsorption removal of ciprofloxacin by gamma ferric oxide and ferrites co-modified carbon nanotubes, J. Colloid Interface Sci. 638 (May 2023) 872–881, https://doi.org/10.1016/j.jcis.2023.02.036.

[114] M.M. Masadeh, K.H. Alzoubi, O.F. Khabour, S.I. Al-Azzam, Ciprofloxacin-induced antibacterial activity is attenuated by phosphodiesterase inhibitors, Curr. Ther. Res. 77 (Dec. 2015) 14–17, https://doi.org/10.1016/j.curtheres.2014.11.001.
[115] N. Ojkic, E. Lilja, S. Direito, A. Dawson, R.J. Allen, B. Waclaw, A roadblock-and-kill mechanism of action model for the DNA-targeting antibiotic ciprofloxacin, Antimicrob. Agents Chemother. 64 (9) (Aug. 2020), https://doi.org/10.1128/aac.02487-19.
[116] H. Zhang, H. Quan, S. Yin, L. Sun, H. Lu, Unraveling the toxicity associated with ciprofloxacin biodegradation in biological wastewater treatment, Environ. Sci. Technol. 56 (22) (Nov. 2022) 15941–15952, https://doi.org/10.1021/acs.est.2c04387.
[117] A. Asadi, et al., Minocycline, focus on mechanisms of resistance, antibacterial activity, and clinical effectiveness: back to the future, J. Glob. Antimicrob. Resist. 22 (Sep. 2020) 161–174, https://doi.org/10.1016/j.jgar.2020.01.022.
[118] R.S. Daum, 115 - *Staphylococcus aureus*, in: S.S. Long, C.G. Prober, M. Fischer (Eds.), Principles and Practice of Pediatric Infectious Diseases (Fifth Edition), Elsevier, 2018, https://doi.org/10.1016/B978-0-323-40181-4.00115-8 (pp. 692-706.e4).
[119] W. Guerra, P.P. Silva-Caldeira, H. Terenzi, E.C. Pereira-Maia, Impact of metal coordination on the antibiotic and non-antibiotic activities of tetracycline-based drugs, Coord. Chem. Rev. 327–328 (Nov. 2016) 188–199, https://doi.org/10.1016/j.ccr.2016.04.009.
[120] M. Wenzel, et al., A flat embedding method for transmission electron microscopy reveals an unknown mechanism of tetracycline, Commun. Biol. 4 (1) (Mar. 2021) 1–13, https://doi.org/10.1038/s42003-021-01809-8.
[121] Q. Liu, et al., Superior adsorption capacity of functionalised straw adsorbent for dyes and heavy-metal ions, J. Hazard. Mater. 382 (Jan. 2020) 121040, https://doi.org/10.1016/j.jhazmat.2019.121040.
[122] A.M. Elgarahy, K.Z. Elwakeel, S.H. Mohammad, G.A. Elshoubaky, A critical review of biosorption of dyes, heavy metals and metalloids from wastewater as an efficient and green process, Clean. Eng. Technol. 4 (Oct. 2021) 100209, https://doi.org/10.1016/j.clet.2021.100209.